TAMPEREEN TEKNILLINEN YLIOPISTO
TAMPERE UNIVERSITY OF TECHNOLOGY

Essi Sarlin

Characterisation of Novel Corrosion Resistant Stainless Steel/Rubber/Composite Hybrid Structures

Julkaisu 1208 • Publication 1208

Tampere 2014

Tampereen teknillinen yliopisto. Julkaisu 1208
Tampere University of Technology. Publication 1208

Essi Sarlin

Characterisation of Novel Corrosion Resistant Stainless Steel/Rubber/Composite Hybrid Structures

Thesis for the degree of Doctor of Science in Technology to be presented with due permission for public examination and criticism in Konetalo Building, Auditorium K1702, at Tampere University of Technology, on the 16th of May 2014, at 12 noon.

Tampereen teknillinen yliopisto - Tampere University of Technology
Tampere 2014

Doctoral candidate:
Essi Sarlin
Department of Materials Science
Tampere University of Technology, Finland

Supervisors:
Associate Professor Minnamari Vippola
Department of Materials Science
Tampere University of Technology, Finland

Professor (Emeritus) Toivo Lepistö
Department of Materials Science
Tampere University of Technology, Finland

Pre-examiners:
Professor Wesley Cantwell
Centre for Materials and Structures
University of Liverpool, UK

D.Sc. (Tech.) Markku Heino
Spinverse Oy, Finland

Opponents:
Professor Wesley Cantwell
Centre for Materials and Structures
University of Liverpool, UK

D.Sc. (Tech.) Tuula Stenberg
Microsoft Corporation, Finland

ISBN 978-952-15-3278-8 (printed)
ISBN 978-952-15-3298-6 (PDF)
ISSN 1459-2045

ABSTRACT

Last decade has shown an increasing interest in hybrid materials and structures. With hybrids there is not only potential to create high strength low weight structures, but also to tailor the properties of the final product in a way that is unattainable by any single material alone. Simpler manufacturing process, increased functional integration, improved sound and vibration damping properties, enhanced crack propagation resistance and protection against collapse in a crash are just some examples of possible advantages of hybrid materials. However, before implementation in industrial application, adequate adhesion between the material components of a hybrid must be ensured. Also, from industrial point of view the required manufacturing method should not increase substantially the costs of the product. Although many established adhesion procedures exist, there is still lack of functioning joining methods for certain material combinations. Especially, the adhesive joining of polymeric materials to stainless steel is demanding, as the conventional methods require laborious manufacturing steps.

In this study, the possibility to bond stainless steel to fibre reinforced epoxy composite with an ethylene propylene diene terpolymer (EPDM) based rubber is studied. Two different rubber compounds are used to create stainless steel/rubber/composite hybrids and a mild steel/rubber/composite structure is used as a reference. Both geometry-dependent peel tests together with environmental testing and geometry-independent single cantilever beam test are used to study the adhesion of the structure's interfaces. Scanning electron microscopy and transmission electron microscopy are used to characterise the nature of the interfaces of the hybrids. In addition, the effect of the rubber on the energy absorption properties of the hybrid structure was of interest. This was studied by non-destructive vibration damping test and by high velocity impact test. In these tests, both sample geometry (rubber thickness) and test parameters were varied to investigate their effect on the hybrid's behaviour.

It was found that the studied method to bond stainless steel and epoxy composite by EPDM rubber enables the use of a simple manufacturing process and it furthermore results in well-bonded hybrid structure. The stainless steel/composite bond strength is defined by the cohesive strength of the rubber and the bond maintains its strength in harsh environments. This enables the evaluation of the stainless steel/composite bond's strength by using the rubber's bulk properties instead of the substrate/rubber interfacial properties, which are difficult to define in a reliable manner. The stainless steel/rubber/composite structure has significantly better vibration damping properties than an all-metal structure. In addition, the rubber improves significantly the damage tolerance of the structure when compared to a corresponding structure which has been conventionally bonded. Thus, the approach of joining stainless steel to fibre reinforced epoxy composite with rubber has potential for industrial applications and the hybrid structure would offer a lighter and better damping solution when compared to all-metallic ones.

PREFACE

The work was carried out in the Department of Materials Science at Tampere University of Technology (TUT). The original idea of stainless steel/rubber/composite hybrid structures was initiated during the project 'Light and Wear Resistant Hybrid Materials - K3MAT' in the Functional Materials program of the Finnish Funding Agency for Innovation (Tekes) in years 2008-2011. However, the research work presented in this thesis was funded by the Doctoral Programme of TUT's President during the period of 2010-2013. Outokumpu Oyj, Rautaruukki Oyj, Kraiburg GmbH and Teknikum Oy are thanked for their co-operation. In addition, the Finnish Foundation for Technology Promotion (TES) and the Research Fund of the City of Tampere are acknowledged for their financial support.

The work was supervised by Professor (Emeritus) Toivo Lepistö and Associate Professor Minnamari Vippola to whom I address my most sincere gratitude. Their guidance, comments and support were essential for my thesis work project. Furthermore, I want to thank Professor Jyrki Vuorinen for his commitment to my work and for the guidance into the world of composites. Also, the work of co-authors Dr. Marian Apostol, Professor Paolo Ermanni, Dr. Laura Frisk, M.Sc. Esa Heinonen, Dr. Maija Hoikkanen, Professor Veli-Tapani Kuokkala, M.Sc. Matti Lindroos, Dr. Yi Liu and Dr. Markus Zogg are acknowledged; the co-operation has been a pleasure and improved the level of my work.

The former and present personnel at the Department of Materials Science and especially the Materials Characterization group deserve my thankfulness for the warm and collaborative working atmosphere. I am grateful to Dr. Mari Honkanen for the endless support, encouragement and fruitful discussions. Also, I want to thank Terho Kaasalainen and the research assistants who have assisted me during my research. In addition, the inspiring and joyful spirit around our coffee table has been a resource during these years.

I want to thank my family and all my friends. The encouragement I have got from my friends has meant a lot to me while the time spend together has been important counterbalance for the work. I also address my deepest gratitude to my parents Erja and Juha and to my sister Aura and to her family for their support and for helping me to keep my feet on the ground. Finally, I want to say my heartfelt thanks to my beloved Mikko, who has always patiently helped me and shared the ups and downs of my work, believed in me unconditionally and expressing his love and care.

Tampere, March 2014

Essi Sarlin

LIST OF PUBLICATIONS

This thesis is based on the original experimental work presented in detail in the following five publications. They are referred to Publications I-V in the text and shown in appendices. In addition, some unpublished data is presented and discussed.

I Essi Sarlin, Esa Heinonen, Jyrki Vuorinen, Minnamari Vippola, Toivo Lepistö: Adhesion properties of novel corrosion resistant hybrid structures, International Journal of Adhesion and Adhesives 49(2014) pp. 51-57.

II Essi Sarlin, Maija Hoikkanen, Laura Frisk, Jyrki Vuorinen, Minnamari Vippola, Toivo Lepistö: Ageing of corrosion resistant steel/rubber/composite hybrid structures, International Journal of Adhesion and Adhesives 49 (2014) pp. 26-32.

III Essi Sarlin, Jyrki Vuorinen, Minnamari Vippola, Toivo Lepistö: The effect of rubber thickness and load rate on the interfacial fracture energy in steel/rubber/composite hybrid structures, Proceedings of the 19^{th} International Conference on Composite Materials (ICCM-19), Montreal, Canada, July 28^{th}-August 2^{nd}, 2013.

IV Essi Sarlin, Yi Liu, Minnamari Vippola, Markus Zogg, Paolo Ermanni, Jyrki Vuorinen, Toivo Lepistö: Vibration damping properties of steel/rubber/composite hybrid structures, Composite Structures 94 (2012) pp. 3327-3335.

V Essi Sarlin, Marian Apostol, Matti Lindroos, Veli-Tapani Kuokkala, Jyrki Vuorinen, Toivo Lepistö, Minnamari Vippola: Impact properties of novel corrosion resistant hybrid structures, Composite Structures 108 (2014) pp. 886-893.

AUTHOR'S CONTRIBUTION

Essi Sarlin is the main researcher and writer of all the publications. She planned and performed most of the experiments and characterisations, analysed the results, and prepared the manuscripts.

In the Publications I-V Professor Toivo Lepistö, Associate professor Minnamari Vippola and Professor Jyrki Vuorinen gave advises on the experimental parts and commented on the manuscripts. In the Publication I Esa Heinonen performed the TEM sample preparation part by FIB. In the Publication II Maija Hoikkanen was responsible for the FT-IR and TGA scans and their interpretation. Laura Frisk contributed to the environmental testing. In the Publication IV the vibration damping test studies were made together with Yi Liu, who also contributed to the interpretation of the results. Markus Zogg and Professor Paolo Ermanni commented on the manuscript. In the Publication V the tests were performed together with Marian Apostol and Matti Lindroos who also processed the high speed camera data. Professor Veli-Tapani Kuokkala commented on the manuscript. All manuscripts were commented on by the co-authors.

LIST OF SYMBOLS AND ABBREVIATIONS

Greek symbols

η	Loss factor
ω_{res}	Resonance frequency
$\Delta\omega$	Frequency range of decay
θ	Impact angle
$tan\ \delta$	Loss tangent

Latin symbols

a	Crack length
C	Compliance
C_0	The intersection of the compliance versus the cubic of the crack length curve with the vertical axis
E	Impact energy
E'	Storage modulus
E''	Loss modulus
E_d	Dissipated energy
E_l	The longitudinal component of the impact energy
E_n	The normal component of the impact energy
F	Input force
G_{Ic}	Critical strain energy release rate in mode I
$G_{I/IIc}$	Critical strain energy release rate in mixed mode I+II
k	Amplitude decay
l	The number of measurement points
m	The slope of the compliance versus the cubic of the crack length curve
m_p	Projectile mass
N	The number of impacts
P	Applied load
R_a	Average profile roughness parameter
Δs	Displacement of a material point
T	Temperature
Δt	Time consumed for a displacement
T_g	Glass transition temperature
v	Velocity
v_i	Initial velocity
w	Specimen width

1,4-HD	Trans-1,4 hexadiene
AISI	American Iron and Steel Institute
ASTM	American Society for Testing and Materials
ATR	Attenuated Total Reflection
BR	Butadiene Rubber
CAI	Compression After Impact
CR	Chloroprene Rubber
Cr	Chromium
DCPD	Dicyclopentadiene
DSC	Differential Scanning Calorimetry
EN	European Norm
ENB	Ethylidene norbornene
EPD	Energy Profiling Diagram
EPDM	Ethylene propylene diene terpolymer (M-type)
FEG-SEM	Field Emission Gun Scanning Electron Microscope
FIB	Focused Ion Beam
FML	Fibre Metal Laminate
FRF	Frequency Response Function
FRF_{mean}	Average frequency response function
FRP	Fibre Reinforced Plastic
FT-IR	Fourier transform infrared
GFRP	Glass Fibre Reinforced Plastic
HVPI	High Velocity Particle Impactor
IIR	Isobutylene Isoprene Rubber
IR	Isoprene Rubber
NBR	Acrylonitrile-butadiene rubber
Ni	Nickel
NR	Natural Rubber
OH	Hydroxyl group
PMH	Polymer Metal Hybrid
RFL	Recorcinol Formaldehyde Latex
RH	Relative Humidity
RMSD	Root-Mean-Square Deviation
ROM	Rule Of Mixtures
RT	Room Temperature
SAM	Scanning Acoustic Microscope
SBR	Styrene-Butadiene Rubber
SCB	Single Cantilever Beam
SEM	Scanning Electron Microscope
Si_3N_4	Silicon nitride
SPS	Steel-Plastic-Steel
TEM	Transmission Electron Microscope
TGA	Thermogravimetric analysis
WC	Tungsten carbide

Contents

1 Introduction

The challenges faced by the engineering industry are nowadays multifold. The ever increasing competition between the companies as well as the strong demand for significant growth in productivity are examples of these tasks. Companies have to develop new product and manufacturing concepts to outdo their competitors. In addition, better usability of products, longer service lives, and concepts that are not easily imitated are in the interest of both manufacturers and customers. Further, the total life cycle of the product including its manufacturing, usage, and recycling, should be as environmental friendly as possible to meet the high standards of today.

Hybrid structures, which may contain several organic and/or inorganic components, combine the best properties of the constituent materials and can solve a wide range of the design challenges of today. Not only high strength or stiffness combined to low weight [1–3], but also other attractive and improved functionalities, such as good damping properties [4–7] and more economical manufacturing processes [8, 9], are potentially achieved with hybrids. The advantageous property combinations of hybrids can lead to valuable outcomes, such as to reductions in energy consumption, to cost efficiency, and to longer service lives.

One of the challenges encountered in the manufacturing and application of hybrid materials is attaining and maintaining sufficient adhesion between the material components. Mechanical interlocking or application of adhesives and primers to create chemical bonding between the adherents are typically used to achieve the required adhesion strength [3]. Especially between materials with very different physiochemical properties, good adhesion with adhesives may require several time consuming manufacturing steps, which increase the costs of the product and thus dilute the attractiveness of the hybrid structure. Thus, new economic methods to produce hybrid materials are needed.

Especially when implementing new structures or new manufacturing methods into an industrial application, the fundamental understanding of the structure's behaviour is essential. In the case of hybrid materials, the knowledge of the structure's interfacial properties and phenomena is not only needed to evaluate whether the structure is suitable for the application but it is also the key to develop the component further in a controlled manner and to simulate its behaviour in different loading environments without large-scale testing. The interfacial data can be achieved by mechanical testing and detailed microstructural characterisation.

The main objective of this thesis is to develop novel corrosion resistant hybrid structures for shell structures, which are not the actual load-bearing components. Examples of this kind of structures are, e.g. engine covers or other protective shells. Especially in heavy machinery, these parts are traditionally all-metal components. The shell structures are typically exposed to impacts and vibrations in fluctuating atmospheres.

In this study, a new approach to join stainless steel and glass fibre reinforced epoxy composite with rubber is investigated. In addition, the aim is to gain in-depth knowledge and understanding of the interfacial properties of hybrid materials of this kind. The microstruc-

tural analysis and the mechanical tests are performed side-by-side to learn the causalities. The steel/rubber/composite hybrids are studied from two aspects: from the adhesion point of view and from the energy absorption point of view.

The thesis comprises eight chapters including this introduction. Chapters 2 and 3 create the theoretical background for the current study. They present and discuss different hybrid structures in general (Chapter 2) and the most commonly used adhesion methods in hybrid structure manufacturing (Chapter 3). Chapter 4 states the research questions and summarizes the main aims and findings of the present study. Chapter 5 starts the experimental part of the thesis and introduces the materials and manufacturing methods as well as the characterisation and test procedures used to create and investigate the steel/rubber/composite hybrids. Chapter 6 reports the main results in detail whereas in Chapter 7 the results are discussed. Chapter 8 describes the concluding remarks. At the end, the five publications that present the original experimental work of this thesis are in the appendix.

2 Polymer/metal hybrid structures

The definition of the word *hybrid* has not yet been established in a way as the word *composite* has. Instead, *hybrid* is perceived to cover a wide range of materials. Ashby defines hybrid materials as "combinations of two or more materials, or of materials and space, assembled in such a way as to have attributes not offered by any one material alone" [1]. However, this definition includes the composite materials within hybrids. In this thesis, the definition separating composites and hybrids or hybrid structures is the following: a composite structure can be regarded as a homogeneous material in a macroscopic scale, whereas in a hybrid structure the behaviour of individual components and the components' interfaces cannot be merged to one unity. This is schematically illustrated in Fig. 2.1.

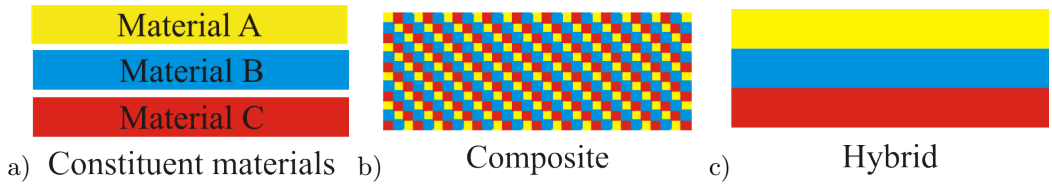

Figure 2.1: *A schematic presentation of (a) three individual material components A, B and C, (b) a composite consisting of materials A, B and C, (c) a hybrid consisting of materials A, B and C.*

Similarly to the composite structures, the most typical and primary advantage of polymer/metal hybrids is weight saving through improved specific strength or stiffness [2]. Thus, polymer/metal hybrids are used, among others, to replace all-metal components. The term *specific* in this context means that the magnitude of a variable has been divided by the material's density and thus it is proportioned to its weight. However, examples of other advantages of hybrids are simpler manufacturing process [9] and increased functional integration [10], improved sound and vibration damping properties [5] as well as enhanced crack propagation resistance [11] and protection against collapse in a crash [12]. Further, the possibilities of hybrids to extend the property space of monolithic materials are numerous.

Within polymer/metal hybrids, traditional metal component materials are aluminium and mild or high strength steel whereas a large variety of polymer grades is applied. The selection of the employed material components depend strongly on the application of the final product. Next, different types of frequently used polymer/metal hybrid structures are introduced.

One of the best-known polymer/metal hybrids is the group of fibre metal laminates (FMLs), which are low weight hybrid laminates used mainly in aeronautical applications. FMLs consist of thin layers of metal sheets and fibre reinforced polymer prepregs. FMLs are generally known for their excellent crack growth resistance under cyclic loading since the interfaces in the structure prohibit effectively crack growth [11]. In addition, the mechanical properties of FMLs are improved by the fibre bridging mechanism of the composite layers where the intact fibres are capable of carrying the additional load in the structure [11]. A 10-100 times

slower crack growth rate has been found for FMLs when compared to pure metals [13]. Most commonly utilized commercial FMLs are aluminium based Glare (aluminium and glass fibre/epoxy composite) and Arall (aluminium and aramid fibre/epoxy composite) but also other material possibilities have been investigated: carbon fibre reinforced thermosets [14] and thermoplastic based composites [15] as well as advanced high strength steel [15], stainless steel [16] and titanium [17] have been implemented into FML structures.

Outside aeronautical applications, different polymer/metal structures are widely used in automotive industry, e.g. in fenders, doors and interior parts as well as in some mechanical components [5, 18–20]. Also, the building sector is using polymer/metal structures, e.g. in roof, air duct and stair structures and in domestic electrical equipments as sound and vibration dampers [21, 22]. Such names as polymer metal hybrid (PMH), laminated steel and steel-plastic-steel (SPS) have been established for polymer/metal hybrids.

Plastic metal hybrids, as called by the company Lanxess, or polymer metal hybrids, as called in many articles (e.g. [23, 24]), are known as PMHs and are used in automotive body-in-white components. PMHs are not necessarily laminates and the adhesion mechanisms between the components may vary [23]. Typically, the metal component in a PMH is mild or high strength steel or aluminium [23, 25]. The main benefits of PMHs, when compared to traditional automotive parts, are the reduced number of components, ready-to-assemble components, weight reduction, additional freedom in design, the improved safety of the vehicle and improved damping properties [8], to name a few. However, the use of PMHs introduces a challenge of recyclability of the components [26].

Laminated steel is a sandwich structure of two steel sheets and a thin polymer core and it is known, e.g. by the trademark names "Quiet Steel" and "Noiseless Steel" [5, 6]. Laminated steel has been designed to reduce vibration and noise in automotive parts. The thickness of the components and thus the frequency range where the material attenuates noise and vibration most effectively can be altered [5]. Laminated steel is used among others in cowl panels, lower plenums, storage tubs, and even in some mechanical parts such as in oil pans [5]. Laminated steel is fully recyclable and it can be formed like plain steel sheets [5].

Steel-plastic-steel (SPS) laminates differ from the laminated steel by a thicker core [27], although the nomenclature is not very clear in all cases. For example, Huang and Leu have studied a SPS structure with a very thin elastomer core [19]. Typical core materials in SPS laminates are polypropylene and fibre reinforced epoxy composites [27]. The main objective of the SPS structures is to maintain the high bending stiffness of metals with lower weight, but other beneficial characteristics of SPSs are better sound and vibration damping properties, better surface finish when compared with other lightweight solutions, as well as improved thermal insulation properties [7, 18, 19, 27, 28]. Also, SPS can be machined with traditional workshop practices [7], but the joining of these structures is difficult [27]. The main drawbacks of the SPS structure are the geometrical distortions and defects arising from the forming processes, especially in the case of bending [18, 19]. Examples of commercial SPS materials are Hylite (aluminium based) [20, 29], Bondal (available in a variety of steel grades) [20, 30] and Sollight (galvanized steel based) [7].

Another widely used class of polymer/metal hybrids are the rubber/steel structures. Due to the viscoelastic nature of rubbers, these structures exhibit outstanding energy absorption behaviour and are used in vibration damping and shock absorption applications [4]. In ad-

dition to the heavy rubber/steel sandwich structures, rubber can also be used to enhance the properties of lightweight fibre reinforced plastic (FRP) structures. FRPs have some disadvantages such as poor damping and impact properties, and a cold haptic feeling [12]. By introducing rubber in FRP structures, the aforementioned properties can be improved without notable addition in weight [12, 31, 32]. In addition, rubber can prevent the collapse of the structure in a crash [12]. Examples of different types of polymer/metal hybrids and their typical applications are shown in Fig. 2.2.

Figure 2.2: *Examples of polymer/metal hybrid structures and their applications: (a) a fibre metal laminate for aeronautic applications [33, 34], (b) a polymer metal hybrid car front end [35, 36], (c) a steel-plastic-steel structure for construction applications [7], (d) a rubber/steel vibration damper for noise control and protection from forces generated in compression [37, 38].*

The most commonly used metals in different polymer/metal hybrid structures are mild and high strength steels and aluminium. Aluminium offers good corrosion resistance but it cannot rival steel in mechanical properties, whereas mild and high strength steels do not meet the corrosion resistance requirements in harsh environments. The use of stainless steel would introduce both good mechanical properties and very good environmental resistance, but the joining of polymers to stainless steel is a demanding task. If a good quality bond between a polymer and stainless steel is achieved, the environmental resistance of the bond is still critical. For example, van Rooijen *et al.* have studied possibilities to use stainless steel in FML structures [16]. They achieved sufficient adhesion level between stainless steel and thermoset by grit blasting but the durability of this bond in different environments was not verified [16]. Also Bähr *et al.* studied several commercial adhesives for glass/stainless steel bonding and they found that only one urethane acrylate based adhesive led to good adhesion strength [39]. However, the shear strength of the joint decreased to less than a half of the initial value during steam exposure [39]. Thus, there appears to be no established economic methods to join stainless steel to polymeric materials in an environmentally resistant way.

3 Adhesive bonding in polymer/metal hybrids

In hybrid structures, the integrity of the joints determines the success of the hybrid. The different bonding mechanisms can be classified into adhesively bonded and into mechanically fastened ones. For laminar structures, adhesive bonding is a natural choice. The advantages of adhesive bonding over mechanical joints are good fatigue resistance due to the large bond area, light weight, insulation, improved damping properties, protection against corrosion and resistance to crack propagation [3]. On the other hand, the possible drawbacks of adhesively bonded joints are complicate fracture mechanisms in the interface, difficulties to predict and detect the bond quality and strength as well as problems related to the joint geometry optimization [3].

Joining adhesively as dissimilar materials as metals and polymers is always a complicated process due to the differences in their chemical and physical properties. Even though the chemical properties, such as polarity and surface energy, would allow the creation of an initial adhesive bond, differences in physical properties, e.g. in ductility or in thermal expansion, may result in the breakage of the joint under the service environment of the structure's application. Thus, it is essential to ensure the durability of the joint between the components of a hybrid structure. In this chapter, aspects of adhesive bonding of polymer/metal hybrid structures are discussed.

3.1 Conventional adhesion procedures

A conventional method to join surfaces adhesively contains the following steps: pre-treatments of the substrates, application of primer(s) and/or adhesive(s), joining the parts together under pressure, and curing the adhesive [2]. The pre-treatments remove possible impurities from the substrates, alter the surface topography to enable mechanical interlocking, and increase the surface area. In the case of metal substrates the pre-treatments are also used to change or to remove the oxide layer. Primers are used to enhance the bonding between the substrate and the adhesive that create the bond between the substrates. Primers and adhesives have to be chosen according to the substrates in question, although the process typically relies on experience since the fundamental nature of the adhesion between organic adhesives and inorganic materials is not well established [40].

When joining two materials adhesively, it should be noticed that the surface properties of a material may differ from its bulk properties. Because of the reactivity of metal surfaces, they are typically covered with native oxide layers, which, for one, can react with humidity and become hydrated [41]. For example, the native oxide layer of AISI 304 stainless steel consists of chromium oxides and hydroxides and has a thickness of 0.5-5 nm [42]. The physiochemical properties of this oxide layer are not similar to the steel's bulk properties. Thus, it is rather the structure and the composition of the oxide layer than the metal's bulk properties that define the surface and the adhesion properties. Usually, thermoplastic polymers are non-polar and hydrophobic and thus difficult to adhere to polar and hydrophilic oxidized metal surfaces [43] whereas the thermosetting polymers, such as epoxy, are more polar and

easier to adhere. In addition, the effect of pre-treatments on the metal surface should be taken into account.

Both mechanical and chemical pre-treatments are used for metals and typically the aim is a clean, easy to wet surface having a sharp and irregular topography [44]. For stainless steel, Cognard recommends electrochemical anodisation as the most effective pre-treatment prior to polymer bonding [40]. Phosphate conversion coatings [45], combinations of acid etching and hydrogen pre-treatments [46], nitric or sulphuric-chromic acid treatments [47] as well as wet and grit blasting [16, 44] have also led to good adhesion properties. After the pre-treatment metal surfaces are typically cleaned with a solvent to remove possible remnants and impurities. The need for the pre-treatment of polymer surfaces depends on the polymer grade and on its surface properties. Among composite structures, the surfaces are typically roughened by mechanical abrading (e.g. grit blasting) [48] or by a peel ply [49] prior to adhesion.

Examples of commonly used primers and adhesives for polymer/metal interfaces are metallic coagents, silanes and cyanoacrylates [16, 44] and a large variety of commercial grades are available. The primer and the adhesive are chosen according to the material combination in question. An alternative for primers and/or adhesives is to coat the substrate with a material that has better adhesion properties to the other adherend [16]. However, if coatings are used to improve the adhesion properties of the substrate, the substrate/coating adhesion has to be verified to be good enough.

The drawbacks of the conventional adhesion processes are the time and the costs required for the application of pre-treatments, primers and adhesives. In addition, chemical pre-treatments may involve the use of toxic and hazardous chemicals, which under the ever tightening national and international regulations are wanted to be avoided. Thus, it would be beneficial if the need for the pre-treatments could be minimised and if the unavoidable processes would be cost-effective. This emphasizes further the need for new approaches to join polymers and metals in a reliable way.

3.2 Rubbers as adhesives

Rubber materials are complicated mixtures of polymers and additives and the properties of a rubber grade are highly dependent on the compound and on its manufacturing process [50]. This is why general values for the properties of different rubbers are difficult to find in the literature. However, when compared to other material grades rubbers have unique properties: extremely high elasticity combined with almost complete recovery and incompressibility [50].

The basis of a rubber grade is the polymer or the polymer mixture. Additives are used to improve the processability and the physical and chemical properties of the compound. The concentrations of the additives may vary remarkably depending on the particular compound but their total weight can easily exceed the total concentration of the polymers. The commonly used additives are, e.g. vulcanising agents, fillers, plasticizers and process oils. Most commonly, sulphur or peroxides are used as vulcanising agents [51], which contribute to the crosslinking of the polymer chains. Together with the vulcanising agent, accelerators, activators, inhibitors and antireversion agents are added to the compound to control the rate of the cure and to help to reduce the property loss due to over cure [51]. Fillers

are used as rubber extenders to decrease the price of the final product but they can also act, e.g. as strengthening agents or as pigments, as does carbon black [51]. Plasticizers, such as paraffin oil, improve the physical properties of the rubber by decreasing the glass transition temperature T_g of the compound [51]. Process oils, e.g. cycloparaffins, facilitate the mixing of the rubber, rubber flow to the mould and mould release, and they can improve the physical properties of the rubber (e.g. elongation at break or tear strength) [51–54].

In addition to the aforementioned additives, there are numerous other chemicals that can be added to the rubber compound to improve its properties or to enhance the processing of the compound. *Internal adhesion promoters*, which improve the rubber adhesion to substrates, are an example of these additives. Since 1930's recorcinol formaldehyde latex (RFL) dipping of tyre cords has been used to enhance the tyre cord/rubber adhesion [55]. Later in 1960's the RFL dip components were added directly to the rubber to form a self-bonding rubber compound [44]. Also, the use of cobalt salts as internal adhesion promoters has been studied since 1950's [44]. More recently, metallic coagents have increased their popularity as internal adhesion promoters in rubbers.

Metallic coagents are metal salts of acrylic or methacrylic acids and their use to improve the effectiveness of peroxide crosslinking has been a common practice for many years [44]. Metallic coagents have been found to have such advantages in a rubber compound as improved tensile strength (at the expense of elongation), low odour, high thermal stability, good dynamic properties, fluid resistance and scorch protection [44, 56]. However, decrease in environmental resistance of rubber due to metallic coagents is reported [44]. Metallic coagents have also been shown to improve the adhesion properties of rubber to other materials and thus they can be used as internal adhesion promoters [44, 56]. Examples of commercial metallic coagents which are used as internal adhesion promoters are Ricobond® 2031 [57], Saret® SR633 [58], and Dymalink® 633 [59].

The advantage of self-bonding rubber grades is naturally the simplified manufacturing process since there is no more need for the application of an adhesive between the substrate and the rubber. The drawbacks of a self-bonding system are the possible unwanted changes in the physical properties of the rubber due to the adhesion promoter and the difficulties in the manufacturing process: the good adhesion properties cause the rubber to adhere also to the mould [44]. Nevertheless, the remarkably less time-consuming and the more straightforward process make the internal adhesion promoters attractive to be used in industrial applications.

For adhesive purposes, rubbers are used in latex based glues (rubber cements), in tapes for electrical insulation and sealing applications, and in elastomer adhesives as an additive [60, 61]. Rubber based adhesives are common and it is estimated that one third of the adhesives used annually are natural rubber (NR) based ones [62]. However, at least according to the writer's knowledge, rubbers as such have not been used as adhesives between dissimilar material components of hybrids in structural applications. Still, due to the possibility to compound rubbers with internal adhesion promoters to be compatible with metals and with polymeric materials, rubbers have potential to be used in polymer/metal hybrid structures. Further, the energy absorption properties and the elasticity of rubbers can improve the dynamic and acoustic properties of the hybrid and equalize residual stresses between the polymeric and the metal components. Thus, a simple manufacturing process and improved mechanical properties can be achieved.

3.3 Classification of rubbers

Rubbers are classified in natural and synthetic grades. Natural rubber is made from organic latex, which is a colloidal caoutchouc dispersion, whereas synthetic rubber grades have been synthesized from petroleum byproducts [63]. Natural rubbers have high tensile strength, high rebound elasticity, very good low temperature flexibility, excellent dynamic properties and very low heat build-up whereas the properties of the synthetic rubbers vary more radically depending on the rubber grade [63]. World total rubber consumption in 2012 was around 26 million tonnes, 57.6% of which was synthetic rubber [64]. The most commonly used synthetic rubber grades are butadiene rubber (BR), chloroprene rubber (CR), ethylene propylene diene terpolymer (EPDM), butyl rubber (IIR), isoprene rubber (IR), acrylonitrile-butadiene rubber (NBR) and styrene-butadiene rubber (SBR) [63]. The highest amount of synthetic rubbers is used in tyre applications.

Among different synthetic rubber grades, EPDM is the most popular grade in non-tyre applications: EPDM had a share of 8% within the synthetic rubber production and a share of 5% within the whole rubber production worldwide in 2011 [64, 65]. As its name states, EPDM consists of ethylene, propylene and diene monomers (Fig. 3.1), which are distributed statistically along the polymer chain [52]. The properties of an EPDM rubber depend on the ratio of the monomers and on the type of the diene [63]. Typically, the concentrations of ethylene and diene are 45-85 mol-% [63] and 1.5 mol-% [52], respectively. The most commonly used diene types in EPDM rubbers are dicyclopentadiene (DCPD), ethylidene norbornene (ENB) and trans-1,4 hexadiene (1,4-HD) [52]. In addition to the monomer concentrations, the EPDM rubber properties depend on the additives as well as on the vulcanising process used [63].

In comparison with other synthetic rubbers, EPDM rubber characteristics are good mechanical properties and high resistance to light, ozone, weather, temperature and several chemicals [63, 66]. Thus, it is typically classified to special-purpose category [52]. Typically, the usable temperature range of EPDM rubbers is -60...160 °C depending on the crosslinking agent (sulphur or peroxide) [67], but may vary due to the compounding and vulcanising. The saturated backbone of the EPDM polymer, i.e. the absence of double bonds in the polymer chain, is the reason for its stability in harsh environments [52]. However, the resistance of EPDM rubbers to aliphatic, aromatic, or chlorinated hydrocarbons is poor [52] and thus the use of EPDM rubbers should be avoided in applications that require constant

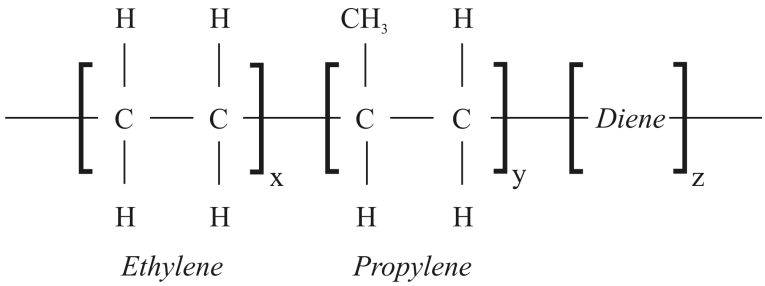

Figure 3.1: *Ethylene, propylene and diene monomers comprising EPDM rubbers. In the polymer chain, there are x ethylene, y propylene and z diene units according to their concentrations. The monomers are distributed statistically along the polymer chain.*

contact of the rubber with oils.

Due to its outstanding ageing resistance [66] and easy-to-adhere nature [44], EPDM rubber is a good choice to be used for adhesive purposes if compounded with internal adhesion promoters. In addition, EPDM rubbers tolerate extremely high levels of fillers and plasticizers without losing their properties, which increases their attractiveness further among other rubber grades [52]. Thus, EPDM rubbers were chosen for this study where their potential to be used as an adhesive between stainless steel and epoxy based composite is studied.

4 The aim of this study

The aim of this study was to investigate the possibilities of EPDM based rubbers to be used as adhesive layer between stainless steel and glass fibre reinforced epoxy composites. The following research questions were stated:

1. Can EPDM based rubber be used as an adhesive layer between stainless steel and epoxy composite?
2. Does the bonding endure harsh environments which can be met in industrial applications?
3. How does the rubber affect the energy absorption properties and damage mechanisms of the hybrid structure?

These questions were investigated by preparing steel/rubber/composite samples. The nature of the interfaces were studied by scanning electron microscopy and transmission electron microscopy and the adhesion properties by adhesion tests. Samples were exposed to harsh environments to study the environmental resistance of the structure. The energy absorption properties and the damage mechanisms of the structure were studied by non-destructive vibration damping test and by high velocity impact test. The research results were published in international refereed journals and in the proceedings of international conferences. The structure of the present study, the publications (I-V) and the most important aims and findings are summarized in Fig. 4.1.

The scientific contributions of the thesis are the following:

- The work describes a novel method to join stainless steel and glass fibre reinforced epoxy composite by EPDM based rubber. This manufacturing method is more simple and environmentally friendly than the conventional joining processes.
- It was found that the method do not require any pre-treatments for the substrates and leads to good, environmental resistant joint between stainless steel and composite.
- In addition, the studied method showed to result in improved damage tolerance when compared to a glued structure and better vibration damping properties when compared to an all-metal structure.

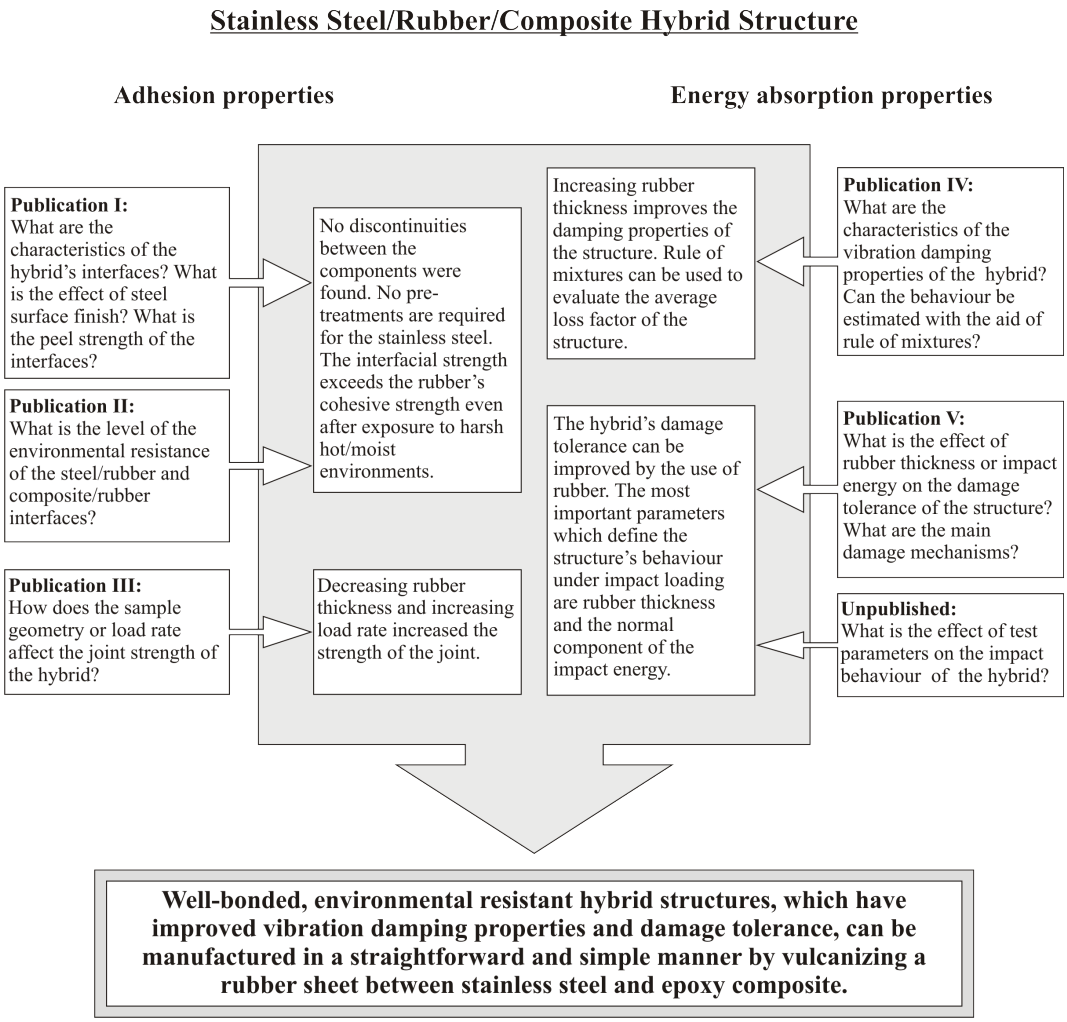

Figure 4.1: *Summary of the present study, its main aims and findings and the related publications (I-V).*

5 Experimental procedures

This chapter introduces the materials and the methods used in the present study. First, the components of the studied steel/rubber/composite hybrid structures are described followed by a brief clarification of the hybrids' manufacturing process. The characterisation methods are reported in the second part of the chapter.

5.1 Materials

Steels

In this study, the main aim was to investigate corrosion resistant polymer/metal hybrid structures for industrial applications. Thus, stainless steel was chosen for the metal component. However, since adhesively bonded stainless steel/polymer hybrid structures are still uncommon, mild steel was used as a reference material. The steel grades used were austenitic Cr-Ni stainless steel grade AISI 304 from Outokumpu Stainless Oy, Finland, and ferritic cold rolled mild steel EN 10130 DC01 from Rautaruukki Oyj, Finland. These particular steel grades were chosen due to their popularity and versatility. AISI 304 steel is the most commonly used stainless steel grade, the classic 18/8 for general purposes [68]. AISI 304 has a wide range of applications in architecture, food processing, domestic sinks and tubs and deep drawing applications [68]. The mild steel grade is also a commonly used steel grade applied, e.g. in housings and in frames [69].

Five different surface finishes for the stainless steel were used in the studies: three industrial finishes, an industrially polished and a sand blasted one (Table 5.1). The as-received surfaces 2B, 2D and 2J are also defined in the standard EN 10088-2. AISI 304 with the surface finish 2B is one of the most frequently used stainless steel [70]. The 2B, 2D and 2J finishes were used in the as-received stage of the manufacturer. The industrially polished (IP) surface was originally a 2D surface that was electrolytically polished by SpecialSteelStudio, Finland. Similarly, the sand blasted (SB) surface was originally a 2D sheet treated in-house with aluminium oxide sand blasting medium (grit 36, average particle size 483 μm). The mild steel was passivation treated by its manufacturer similar to the grades used as industrially coated. The aim of the passivation treatment is to enhance the adhesion properties of the steel but the procedure is not public. It is possible that the passivation treatment changes the mild steel surface topography in some extent.

The thickness of the steel sheets was 0.5 mm, but in the adhesion tests a 4 mm thick flat bar iron stiffener was glued on the back side of the metal component to prevent its bending during testing. The densities of the stainless steel and the mild steel are 7900 kg/m^3 and 7850 kg/m^3, respectively [69, 70].

Rubbers

Three different ethylene propylene diene terpolymer (EPDM) based rubber grades were used in the study. EPDM is a commonly used synthetic rubber in non-tyre applications, con-

Table 5.1: *The steel surface finishes used in the study.*

Steel grade	Surface finish	Code	Reference
Stainless steel	*Cold rolled, heat treated, pickled, skin passed*	*2B*	[70]
	Cold rolled, heat treated, pickled	*2D*	[70]
	Dry brushed	*2J*	[70]
	Industrially polished	*IP*	
	Sand blasted	*SB*	
Mild steel	*Cold rolled, passivation treated*	*CR*	[69]

sisting of ethylene, propylene and diene monomers [63–65]. Typical applications of EPDM rubbers are automotive applications (e.g. shock absorbers, profiles and weather strips), electrical applications (e.g. cable insulation and jacketing of electrical cables), and building and construction applications (e.g. roofing membranes and seals) [52, 63, 71], to name a few.

The EPDM based rubbers bonded to the steel and the composite surfaces in this study were manufactured by Teknikum Oy, Finland (grade A) and by Kraiburg GmbH, Germany (grades B and C). The grade A has a trade name Teknikum TRA10 and its ingredients are EPDM rubber, ZnO, stearic acid, polyethylene wax, carbon black, paraffin oil, internal adhesion promoter and peroxide. The grade B is also designed for stainless steel whereas the grade C is designed for mild steels. The main components of rubbers B and C are EPDM rubber, silica (rubber B) or carbon black (rubber C), paraffin oil, internal adhesion promoters, silane, curing promoters, and peroxide. The densities of the rubbers are 1240 kg/m^3, 1130 kg/m^3, and 1110 kg/m^3 for rubbers A, B, and C, respectively [Publication IV]. The glass transition temperatures of rubbers A, B and C are -38 °C, -45 °C, and -50 °C (at 1 Hz).

Composite

The glass fibre reinforced plastic (GFRP) composite sheets were manufactured in-house by vacuum infusion from stitched 0/90 E-glass fibre fabrics (682 g/m^2, from Ahlstrom Oyj, Finland) and Sicomin SR 1660/SD 7820 epoxy (from Sicomin Composites, UK). The epoxy was cured according to the following cycle: 48 h @ RT + 8 h @ 60 °C + 4 h @ 90 °C + 4 h @ 120 °C + 4 h @ 150 °C. This curing cycle leads to a glass transition temperature of 150 °C [72]. The nominal thickness of the composite sheets was 3.5 mm consisting of 6 layers of fabrics. The fibre content of the composite was about 46 vol-% and the density 1760 kg/m^3 [Publication IV]. The heat resistant epoxy was chosen to provide resistance to the vulcanising temperature of the rubbers (130 °C). The cure of the composite layers was done separately before rubber vulcanisation because the different vulcanising conditions of the rubber grades could have caused deviation in the curing process of the composite.

Manufacturing of the hybrids

In this study, the amount of pre-treatments was wanted to be minimised. To remove oil and grease residues from the steel surfaces, they were rinsed with acetone and ethanol before the rubber bonding. This cleaning procedure is fast and uncomplicated when compared with traditional pre-treatments of metals, such as electrochemical anodisation or grit blasting. In this thesis, the word *as-received* refers to an industrial surface finish that has been cleaned in

a simple manner by acetone and ethanol. To roughen the composite surfaces, a HexForce® T470 (Hexcel Co., USA) peel ply was applied during the composite manufacturing. The peel plies were removed from the composite surfaces just prior to the rubber bonding. The rubbers were delivered by the manufacturers as calendered sheets, which were applied as they were.

The bonding of the components was achieved during the vulcanisation of the rubber. The vulcanising parameters for different types of samples are shown in Table 5.2. The vulcanising of the rubbers was done according to the manufacturers' guidelines, except for the composite/rubber A samples, for which the lower vulcanising temperature was compensated with longer vulcanisation time. To ensure that a high enough degree of vulcanisation was reached during the composite/rubber A sample vulcanisation, differential scanning calorimetry scans (DSC) were done for rubber A (see Chapter 5.2).

Two types of hybrid samples were manufactured: three component and two component samples (Table 5.2). Basically, the samples consisting either of steel or composite substrate and rubber were suitable for adhesion testing and those consisting of all three components were suitable for vibration damping and impact testing. The sample dimensions for different test methods can be found in the next sub-chapters.

Table 5.2: *The vulcanising parameters for different sample types.*

Sample components			Temperature	Time	Pressure
Steel grade	**Rubber grade**	**Composite**	**[°C]**	**[min]**	**[MPa]**
Stainless steel	*A*	-	*160*	*15*	*1.2*
-	*A*	*GFRP*	*130*	*18*	*1.2*
Stainless steel	*A*	*GFRP*	*130*	*18*	*1.2*
Stainless steel	*B*	-	*130*	*20*	*1.2*
-	*B*	*GFRP*	*130*	*20*	*1.2*
Stainless steel	*B*	*GFRP*	*130*	*20*	*1.2*
Mild steel	*C*	-	*130*	*30*	*1.2*
-	*C*	*GFRP*	*130*	*30*	*1.2*
Mild steel	*C*	*GFRP*	*130*	*30*	*1.2*

5.2 Characterisation of hybrids

Electron microscopy (Publications I-V)

The substrate surfaces, the cross-sections of the hybrids and the peeled surfaces of the steel and composite substrates were studied with field emission gun scanning electron microscope (FEG-SEM) Zeiss ULTRAplus, Carl Zeiss SMT AG, Germany. The steel surfaces did not require any sample preparation whereas the composite and the rubber surfaces were coated with a thin gold layer to ensure good electrical conductivity. Conventional cross-sectional sample preparation method, including cutting the sample from the original test specimens, mounting to epoxy at room temperature, grinding, polishing and carbon coating to ensure the conductivity, was used to investigate the cross-sections of the hybrid structures.

To study the interfaces of the hybrid structures more closely, cross-sectional transmission electron microscope (TEM) samples were prepared. The composite/rubber interfacial samples were prepared by a microtome at room temperature in the Institute of Biotechnology, University of Helsinki, Finland. The glass fibre in the composite prevented the cutting with the thin sectioning method. Thus, plain epoxy/rubber samples were prepared by using a similar epoxy resin system as in the original composite sheets, similar peel ply and similar curing and vulcanisation procedures to attain suitable samples for the thin sectioning. This should not alter the interfacial conditions, since the glass fibres in a well wetted composite are covered with epoxy.

The steel/rubber cross-sectional TEM samples were manufactured by focused ion beam (FIB) method. The sample preparation was started with a traditional cross-sectional TEM sample preparation method: two pieces of steel/rubber samples were cut to the size of approximately 1.5 mm × 1 mm × 0.5 mm and placed rubber sides face-to-face in a titanium grid. The pieces were attached with an epoxy adhesive (Fluka 45359 Epoxy - Embedding Kit), after which the epoxy was cured at 65 °C for 16 hours. The EPDM rubber is assumed to endure the sample preparation temperature without degradation [67, 73]. Then the samples were pre-thinned by hand to a thickness of ∼100 μm. The final TEM samples were made using a FEI Helios Nanolab 600 dualbeam FIB system at the University of Oulu, Finland. A layer of platinum (∼1 μm) was first deposited on the steel/rubber interface as a protection layer with the FIB. The rough TEM sample was then cut out from the bulk material (Fig. 5.1a) and lifted off to the TEM grid with an Omniprobe needle manipulator. After that, the bulk sample was attached to the grid as shown in Fig. 5.1b. The grid was then turned 90° and the sample was thinned from both sides to the final thickness. During the final thinning, the platinum layer was removed. The samples were studied with JEOL JEM 2010 TEM (Jeol, Japan).

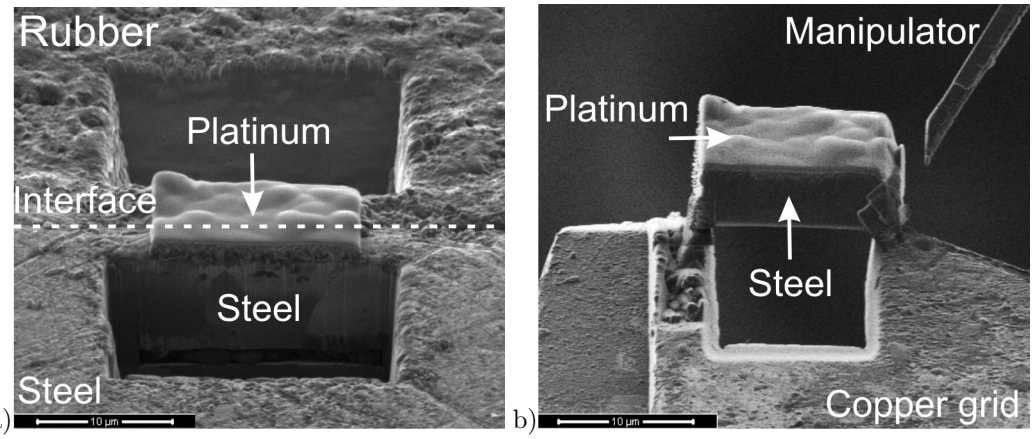

a) b)

Figure 5.1: *Figure (a) shows a steel/rubber bulk sample from which the interfacial TEM sample is cut by FIB and in figure (b) the sample is in the FIB grid. Before examination with TEM, the sample was turned so that the interface is parallel to the TEM electron beam. [Publication I]*

Surface roughness measurements (Publication I)

The surface roughness of the substrates was studied with Laser profilometer (UBM-Microfocus Compact, NanoFocus AG, Germany). The average surface roughness parameter R_a was measured from a length of 50 μm in two perpendicular directions, longitudinal and transverse to the rolling direction of the steel. The reported R_a values are the averages of the transverse and longitudinal R_a values.

Adhesion test set-ups (Publications I-III)

Methods to study the adhesion of rubber to rigid substrates are described in the ASTM D429 standard, which introduces a method for determining the adhesive strength of rubber/metal bonding. In this test method the rubber is peeled from the substrate at an angle of 90°. However, Cook *et al.* have found that a peel angle of 45° is the optimum for testing rubber/steel adhesion since it directs the fracture into the interface and the cohesive fracture of rubber is minimised [74]. Thus a floating roller peel test configuration (Fig. 5.2, also introduced in the standard EN1464) was used. The peel test geometry provides a constant peel angle of 45°. In general, peel tests are widely applied to study quickly and effortlessly the mechanical load endurance of an interface.

The peel test samples (size 100 mm × 12 mm) were cut from the larger steel/rubber and the composite/rubber laminates by water jetting. A pre-crack was created by inserting a 30 μm thick plastic layer between the rubber and the substrate before vulcanisation. The rubber thickness in the samples was 2 mm. Prior to the peel testing, the samples were conditioned for 72 hours in 23 ± 1°C and 50 ± 2% relative humidity (%RH). The peel tests were performed with a universal mechanical testing machine and with a 1 kN load cell (Messphysik, Austria). The cross head rate was 100 mm/min according to the EN 1464 standard. All reported peel strength values are averages of 5-7 peel test results.

Peel tests provide only geometry-dependent information. To study the effect of rubber thickness and load rate to the adhesion properties of the hybrid structure, a geometry-independent

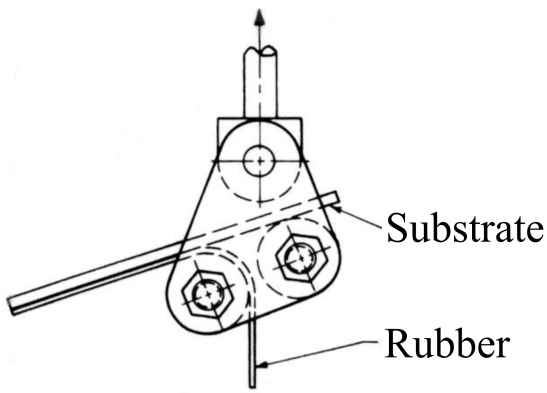

Figure 5.2: *The floating roller peel test geometry, modified from [3], [Publication I].*

test set-up was used. In principle, the geometry-independent test methods provide quantitative results which can be used directly in design codes and in durability models [75]. These test methods introduce opening (mode I), sliding (mode II), or tearing (mode III) mode of fracture in the studied interface, or a mixture of these modes. Generally, the mixed mode I+II is considered to correspond best to most of the realistic situations [76]. The applied test set-up providing this mixed mode I+II loading was single cantilever beam (SCB) test geometry (Fig. 5.3).

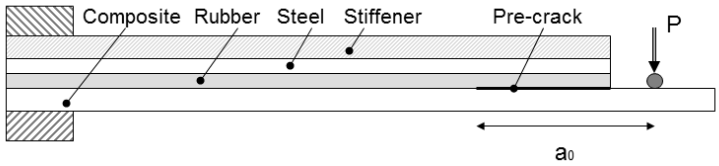

Figure 5.3: *A schematic representation of the single cantilever beam test and sample geometry.*

Only the mild steel/rubber C/composite structure was investigated by the SCB test. A 30 μm thick plastic layer was used to produce a pre-crack in the composite/rubber or in the steel/rubber interface. After extracting the 20 mm $\times$ 180 mm sized samples from larger laminates by water jet cutting, the thicknesses of the rubber layers were verified from cross-sectional samples with optical stereomicroscope Leica MZ 7.5. The tests were performed using a servohydraulic mechanical testing equipment MTS 810 TestStar with a 10 kN load cell.

The SCB tests were performed under displacement control. Three different cross head rates, namely 0.1 mm/min, 1 mm/min and 10 mm/min, were used to study the effect of load rate. To study the effect of rubber thickness on the adhesion properties, three different rubber thickness, namely 0.5 mm, 0.7 mm and 1.6 mm, were used. The propagation of the delamination was observed visually with the aid of a magnifying glass and a grid painted on the both sides of the samples. At least three samples for each sample type and test condition were tested.

The interfacial fracture energy was calculated from the load/displacement data of the servohydraulic testing machine by a compliance calibration method. The method assumes that the relationship between the crack length a and compliance C can be written as [15]:

$$C = ma^3 + C_0 \tag{5.1}$$

where m is the slope of the compliance versus the cubic of the crack length curve. The constant C_0 is obtained from the intersection of the aforementioned curve and the vertical axis. Then, the strain energy release rate $G_{I/IIC}$ can be calculated from Eq. 5.2 [15]:

$$G_{I/IIC} = \frac{3P^2ma^2}{2w} \tag{5.2}$$

where P is the applied load and w is the specimen width.

Environmental testing (Publication II)

There are no established general practices to test the environmental resistance of polymer/metal interfaces. Instead, such issues have been studied in various test environments depending on the material combination and application in question. The combination of the 85 °C temperature and the 85%RH humidity is used in the steady state temperature humidity bias life tests for packaged devices [77]. Also the ASTM D3137 standard for hydrolytic stability of rubbers instructs the temperature of 85 °C above a water container, which is close to the humidity of 85%RH. Thus, the 85 °C/85%RH condition was chosen for this study as well. Here, three sets of peel test samples were aged in different conditions before testing in order to study the environmental resistance of the joint strength. Table 5.3 shows the ageing procedure of the different sets. The EPDM rubbers are assumed to endure these environments without degradation [67, 73]. Between the ageing and the peel testing, all samples were conditioned for 72 hours in 23 ± 1 °C and 50 ± 2%RH. To determine the possible changes in the chemical structure or composition of the rubbers after ageing, Fourier transform infrared (FT-IR) and thermogravimetric analysis (TGA) were performed and the Shore D hardness of different rubber grades was tested. Stainless steel/rubber A/composite samples were also impact tested after exposure to hygrothermal environment.

Table 5.3: *Ageing environments used to study the environmental resistance of the substrate/rubber interfaces.*

Set of samples	Ageing environment
Non-exposed	-
Isothermal environment	*85 °C, ambient atmospheric conditions for 500 hours*
Isohume environment	*25 °C, 85% relative humidity for 500 hours*
Hygrothermal environment	*85 °C, 85% relative humidity for 500 hours*

Structural characterisation of rubbers (Publications I and II)

The degree of vulcanisation of rubber A was verified after the vulcanisation by differential scanning calorimetry (DSC) since the vulcanisation time and temperature had to be changed from the manufacturer's guidelines. The used DSC equipemnt was DSC 204 F1, Netzsch, Germany. The possible changes in the chemical structure or composition of the rubbers after ageing were studied by Fourier transform infrared spectroscopy (FT-IR) and thermogravimetric analysis (TGA). The FT-IR spectra were measured with Tensor 27 from Bruker Optics, equipped with germanium attenuated total reflection (ATR) accessory. For each spectrum 64 scans were collected with resolution of 4 cm^{-1}. Perkin Elmer STA 6000 equipment was used for the TGA studies. For the TGA, 10-20 mg specimens of the rubber grades were heated from 30 °C to 950 °C at a rate of 10 K/min under nitrogen flow of 20 ml/min. Further, Shore D hardnesses of the different rubber grades were measured according to the ASTM D2240 standard before and after each environmental test.

Vibration damping test set-up (Publication IV)

A frequency domain test method was used to study the vibration damping properties of the steel/rubber/composite structures. The frequency domain test was a free hanging plate test,

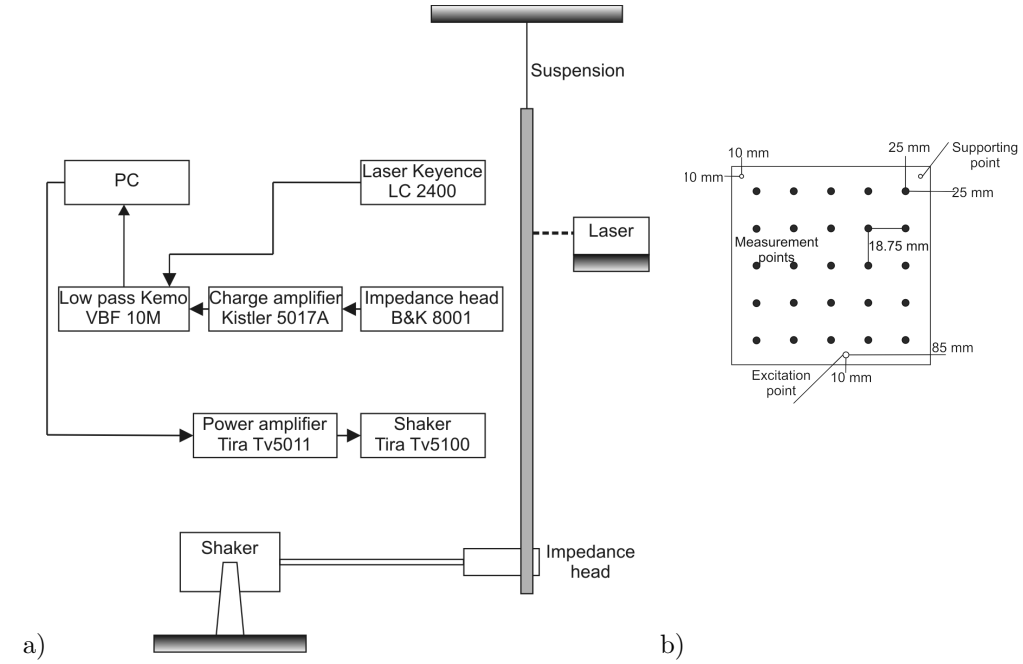

Figure 5.4: *Schematic presentations of (a) the frequency domain test set-up and (b) the measurement, support and excitation points in the samples [Publication IV].*

in which a 200 mm × 200 mm sized plate is suspended with two elastic wires and excited with a shaker (Fig. 5.4a). The shaker was stud-mounted to the specimen and the suspension generates free-free boundary conditions, which is generally accepted to be the only one suitable for complicated structures [78]. A laser was used to detect the displacement of the plate during excitation at the measurement points shown in Fig. 5.4b. The reflectivity of the measurement spots were enhanced by using reflective tape. A detailed description of the test set-up is given in [79] and a similar one is used, e.g. in [80].

The free hanging plate test method enables the evaluation of loss factor only in resonance, i.e. at discrete eigenmode-points starting from the first resonance frequency of the sample. Thus, the first resonance frequency was determined for each sample individually before the actual damping test. Then the specimens were scanned in a frequency range up to 500 Hz with a sine-sweep signal from the 25 measurement spots and the frequency response function (FRF) of the structure's mobility was recorded. To determine the behaviour of the whole plate, a mean frequency response function was calculated with a root-mean-square of the FRFs of the individual measurement points:

$$FRF_{mean} = 20 \cdot log(\sqrt{\frac{\sum_{i=1}^{l} \left|\frac{v}{F}\right|^2}{l}}) \tag{5.3}$$

where l refers to the number of measurement points (l=25), v is the velocity of the studied point and F is the input force of the excitation. In the FRF_{mean} curve, each peak represents a resonance frequency of the plate and the modal loss factor η can be calculated from the peaks with the fractional power bandwidth method:

$$\eta = \frac{1}{\sqrt{10^{\frac{k}{10}} - 1}} \frac{\Delta\omega}{\omega_{res}} \tag{5.4}$$

where k is the amplitude decay of k dB in frequency domain, $\Delta\omega$ is the frequency range of decay in radian and ω_{res} is the resonance frequency in radian. The ASTM E756 standard defines the k to be between 0.5 and 3 dB. The free hanging plate test method is accurate only for structures with small damping values (loss factor up to 0.2-0.3) since in the FRF some peaks will be eliminated by remarkable damping [81].

Impact test set-up (Publication V)

The impact properties of the steel/rubber/composite hybrid structures were tested by high velocity impact test. Several parameters were varied to study the impact properties in an all-round manner. The effect of the following parameters was studied: rubber thickness, impact energy, impact angle, projectile velocity with constant impact energy, the number of impacts, specimen temperature and specimen exposure to harsh environments before the impact.

The impact test equipment was an in-house developed high velocity particle impactor (HVPI). In this device, compressed air is used to fire a 9 mm diameter projectile towards the sample. The velocity of the projectile is determined by a computer controlled pressure reservoir and the projectile velocity before impact is recorded with a commercial ballistic chronograph placed in front of the target assembly. The test set-up allows wide range of impact angles approximately from 10° to 90°. The impact event is recorded with a high speed camera (NAC Memrecam fx K5, NAC Image Technology, USA). The high speed video images were recorded at a constant frame rate varying between 20000-40000 frames per second according to the test. The HVPI equipment complex is fully computer controlled. A schematic representation of the test set-up is shown in Fig. 5.5.

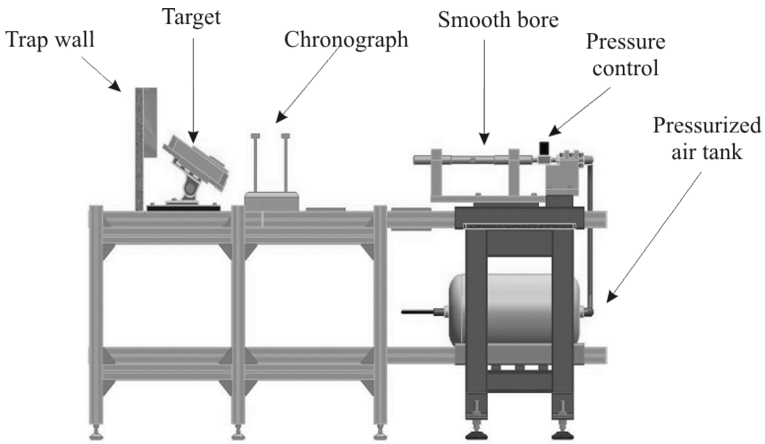

Figure 5.5: *A schematic presentation of the high velocity impact test set-up [82].*

In this study three different ball types were used as projectiles: steel balls (2.98 g in weight), tungsten carbide balls (WC, 5.73 g in weight) and silicon nitride balls (Si_3N_4, 1.25 g in weight). The pressure range used was 1-14 bar and it was adjusted to provide a suitable kinetic energy for the projectiles. Specimen angle was either 30°± 1°, 45°± 1° or 60°± 1°. Impact angles higher than 60° were not used since high energetic projectiles after impact in an angle close to 90° could have caused damage for the test equipment after rebound. When not investigating the effect of impact angle, the specimen angle was set to 45° as a compromise between the two extremes. Some of the samples were heated in oven or cooled in ethanol/liquid nitrogen bath with the sample holder just before the impact to investigate the influence of different sample temperatures. The temperatures of the samples were recorded by type K thermocouples welded to the sample surface and a Fluke 52 II Thermometer. Thus the temperature measured was actually the steel surface temperature and the temperature of the composite layer may have been higher in the hot samples or lower in the cold samples. To study the effect of ageing, some samples were exposed to hot/moist environment (85 °C and 85%RH) for 20 days prior to the impact testing. The peel tests were used to verify the stability of the adhesion properties of this structure during the ageing process. A summary of the test conditions is shown in Table 5.4.

The 50 mm × 50 mm sized samples were fixed with the steel side upwards in a 130 mm × 130 mm aluminium clamp. The clamp had a circular opening of 40 mm in the centre. The geometry enables the sample to bend during the impact. When determining the size of the clamp opening, it was optimized to exceed the size of the maximum damage at the applied maximum energy but simultaneously to minimise the sample material consumption. The round clamp opening was chosen to create a spherical boundary condition. A schematic representation of the clamp and the sample geometry are shown in Fig. 5.6. Three samples were tested per each test parameter combination.

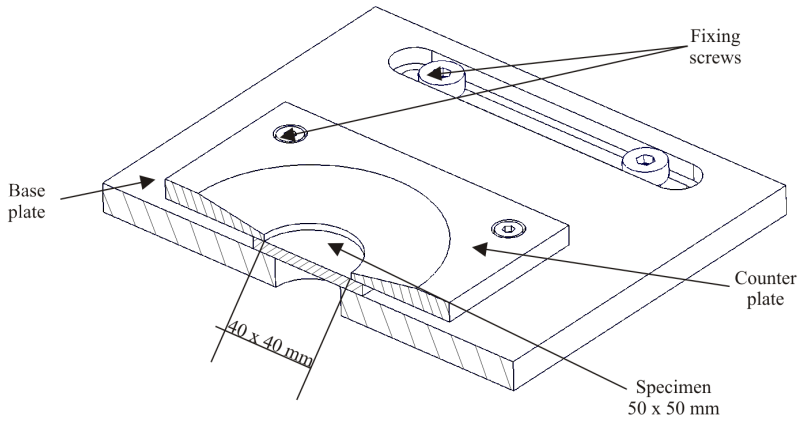

Figure 5.6: *A schematic section view of the impact test specimen and the sample holder [Publication V].*

Table 5.4: *A summary of the impact test parameters. The initial projectile velocity v_i, the impact energy E, the impact angle θ, the sample temperature T, the number of the impacts per sample N as well as information of the possible ageing are included.*

Steel	Adhesive	Composite	Projectile	v_i [m/s]	E [J]	θ [°]	T [°C]	N []	Ageing
To study the effect of rubber thickness									
Stainless steel 0.5 mm	*Rubber A 0.5 mm* *Rubber A 1.0 mm* *Rubber A 1.5 mm*	*GFRP 3.5 mm*	*Steel*	*100*	*15*	*45*	*RT*	*1*	*No*
Stainless steel 0.5 mm	*Rubber B 0.5 mm* *Rubber B 1.0 mm* *Rubber B 1.5 mm*	*GFRP 3.5 mm*	*Steel*	*100*	*15*	*45*	*RT*	*1*	*No*
Stainless steel 0.5 mm	*Epoxy adhesive*	*GFRP 3.5 mm*	*Steel*	*100*	*15*	*45*	*RT*	*1*	*No*
Mild steel 0.5 mm	*Rubber C 0.5 mm* *Rubber C 1.0 mm* *Rubber C 1.5 mm*	*GFRP 3.5 mm*	*Steel*	*100*	*15*	*45*	*RT*	*1*	*No*
Mild steel 0.5 mm	*Epoxy adhesive*	*GFRP 3.5 mm*	*Steel*	*100*	*15*	*45*	*RT*	*1*	*No*
To study the effect of impact energy									
Stainless steel 0.5 mm	*Rubber A 1.0 mm*	*GFRP 3.5 mm*	*Steel*	*44* *100* *142*	*3* *15* *30*	*45*	*RT*	*1*	*No*
To study the effect of projectile velocity									
Stainless steel 0.5 mm	*Rubber A 1.0 mm*	*GFRP 3.5 mm*	*Si_3N_4* *Steel* *WC*	*157* *100* *71*	*15*	*45*	*RT*	*1*	*No*
To study the effect of impact angle									
Stainless steel 0.5 mm	*Rubber A 1.0 mm*	*GFRP 3.5 mm*	*Steel*	*100*	*15*	*30* *45* *60*	*RT*	*1*	*No*

Continued on the next page

Table 5.4 – continued

Steel	Adhesive	Composite	Projectile	v_i [m/s]	E [J]	θ [°]	T [°C]	N []	Ageing
To study the effect of repeated impacts									
Stainless steel 0.5 mm	*Rubber A 1.0 mm*	*GFRP 3.5 mm*	*Steel*	*142* *44*	*30* *3*	*45*	*RT*	*1* *10*	*No*
Stainless steel 0.5 mm	*Epoxy adhesive*	*GFRP 3.5 mm*	*Steel*	*142* *44*	*30* *3*	*45*	*RT*	*1* *10*	*No*
To study the effect of temperature									
Stainless steel 0.5 mm	*Rubber A 1.0 mm*	*GFRP 3.5 mm*	*Steel*	*100*	*15*	*45*	*-25* *RT* *80*	*1*	*No*
To study the effect of ageing									
Stainless steel 0.5 mm	*Rubber A 1.0 mm*	*GFRP 3.5 mm*	*Steel*	*100*	*15*	*45*	*RT*	*1*	*No* *Yes**

*Ageing procedure was 85 °C and 85%RH for 20 days

The dissipated energy E_d of the projectile was calculated by comparing the initial and post-impact kinetic energy of the projectile according to Eq. 5.5:

$$E_d = \frac{1}{2} m_p \left(v_i - \frac{\Delta s}{\Delta t} \right)^2 \tag{5.5}$$

where m_p is the projectile mass, v_i is its initial velocity, Δs is the displacement of a material point in two images and Δt the time consumed for this displacement of the projectile. The incident velocity was measured with the ballistic chronograph placed in front of the sample. A custom image analysis suite was used to estimate the velocity of the projectiles after the impact by overlaying two post-impact images from the high speed photographs, where the projectile is no more in contact with the specimen. Since the spherical shape of the projectile allows tracking of the same material point in the images (the centre of the sphere), the distance travelled by the projectile can be calculated from the overlaid images. Examples of the high speed camera images before, during, and after the impact event are shown in Fig. 5.7.

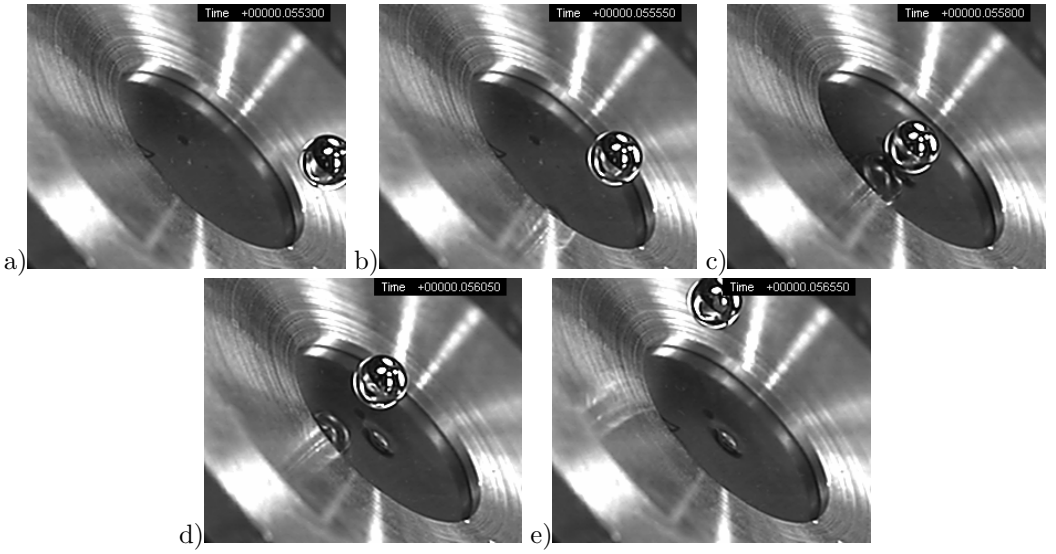

Figure 5.7: *Examples of the high speed camera images: (a-b) the projectile approaches the specimen, (c) the impact event, and (d-e) the projectile moves away from the specimen after the impact.*

A small error is involved in the distance calculations due to a slightly angular position of the camera, but it has a negligible influence on the accuracy of the results and thus it was omitted. The mass change of the projectile during the impact was also assumed to be negligible since the projectile remains intact and has no sign of noticeable wear or increase in mass due to adhesion from the counter-surface.

To study the damages induced by the impacts, the samples were photographed from both sides and the composite damage area values were defined from the images by using an image processing program (similar to Fig. 6.15c). The samples impacted multiple times were photographed after every impact but the samples were not removed from the holder in between

to minimise changes in the impact location. The dimensions of the composite/rubber delamination were possible to evaluate from the photographs due to the translucent nature of the composite, whereas the steel/rubber delaminations were not possible to study by optical means. Non-destructive methods are generally used to evaluate the extent of delaminations in impact loaded composite samples. The original plan was to apply a scanning acoustic microscope (SAM) to find out the dimensions of the delaminations in the steel/rubber interface. However, the multi-layered hybrid structure and the internal structure of the composite layer caused so complex return echoes that even the analysis of the initial, non-damaged samples was not possible. Instead, for all studied test parameter combinations, one cross-sectional sample with intermediate damage area was studied with SEM.

6 Results

In this chapter, the most important results of the attached five publications are presented together with some unpublished data. First, the microstructural electron microscopy and the surface roughness studies are illustrated. Subsequently, the adhesion properties and finally, the results of vibration damping and impact tests are shown. The results are discussed in the next chapter.

6.1 Microstructural characterisation

Substrates

The SEM images of the steel and the composite substrates are shown in Fig. 6.1. The cold rolled mild steel surface is rather even without distinctive grain boundaries. The 2B and 2D surfaces of stainless steel exhibit clearly distinctive grain boundaries, whereas the sand blasted stainless steel surface shows substantially rougher topography. The brushed 2J surface shows oriented brush marks and the industrially polished IP surface is very smooth with some corrosion pits. The composite surface has a regular and rough surface after the removal of peel ply.

The measured R_a values for the different surface finishes are shown in Table 6.1 together with the manufacturers' values for the as-received steel surface finishes. The R_a value reported by the manufacturer for the mild steel is for a grade without the passivation treatment, which may affect the deviation between the values.

Table 6.1: *The studied substrates and their average profile roughness parameters (R_a) measured with laser profilometer (*) and reported by the manufacturer (**), if available. Modified from [Publication I].*

Code	Surface treatment	R_a* [μm]	R_a** [μm]
CR	*Cold rolled, passivation treated mild steel*	*0.43*	*0.6-1.9* [69]
2B	*Cold rolled, heat treated, pickled, skin passed stainless steel*	*0.35*	*0.1-0.5* [70]
2D	*Cold rolled, heat treated, pickled stainless steel*	*0.38*	*0.2-1.0* [70]
2J	*Dry brushed stainless steel*	*0.31*	*0.2-0.4* [70]
SB	*Sand blasted stainless steel*	*2.46*	-
IP	*Industrially polished stainless steel*	*0.39*	-
GFRP	*HexForce® T470 peel ply*	*23.51*	-

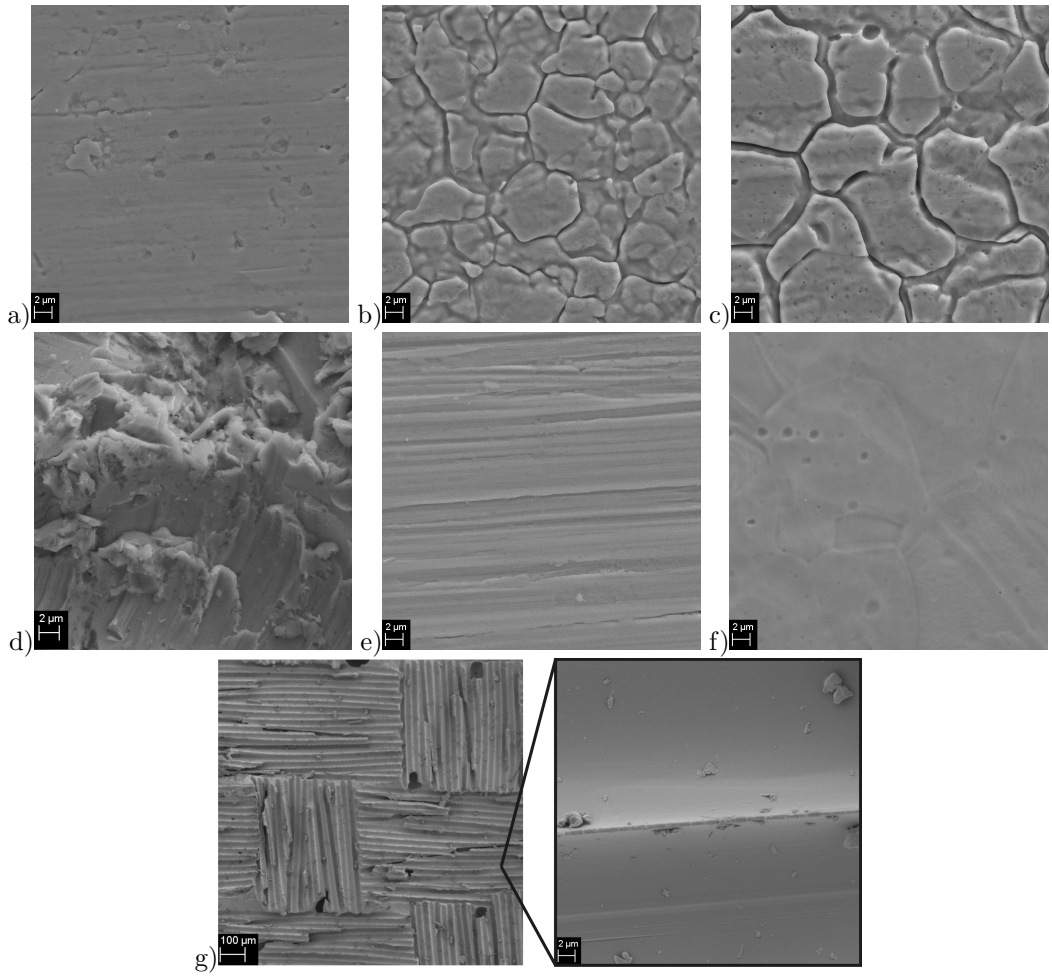

Figure 6.1: *Substrates before rubber bonding: (a) mild steel surface (CR) and the stainless steel surfaces (b) 2B, (c) 2D, (d) SB, (e)2J, and (f)IP. The composite surface is shown in g). [Publication I]*

Hybrid structure

Examples of the SEM cross-sectional images of the hybrid structure are shown in Fig. 6.2. According to the images, there is a good contact between the components. The SEM images revealed also that the flat steel surface provides much less mechanical interlocking and surface area than the coarse and undulating composite surface. However, since it is possible that the rubber has smeared over the interfaces during sample preparation, it is difficult to deduce the true nature of the interface from the SEM images. Thus, despite the much more laborious fabrication, TEM samples were prepared to study the interfaces closer.

In Fig. 6.3 the cross-sectional TEM images from the steel/rubber and epoxy/rubber interfaces are shown. A close contact between the substrates and the rubbers was observed without any discontinuities. In Fig. 6.3d-f the reinforcing particles (carbon black/silica) of the rubbers can be seen as spherical darker areas.

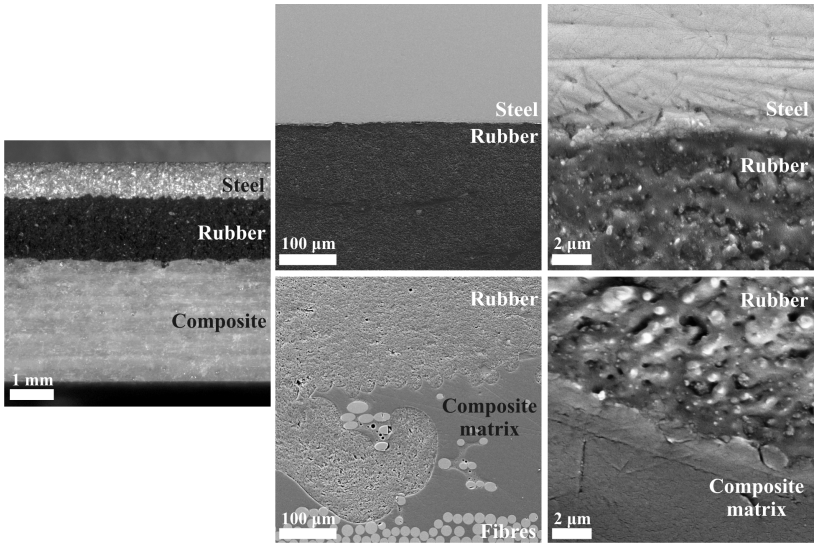

Figure 6.2: *Cross-sectional SEM images of the mild steel/rubber C/composite hybrid structure. Modified from [Publication III].*

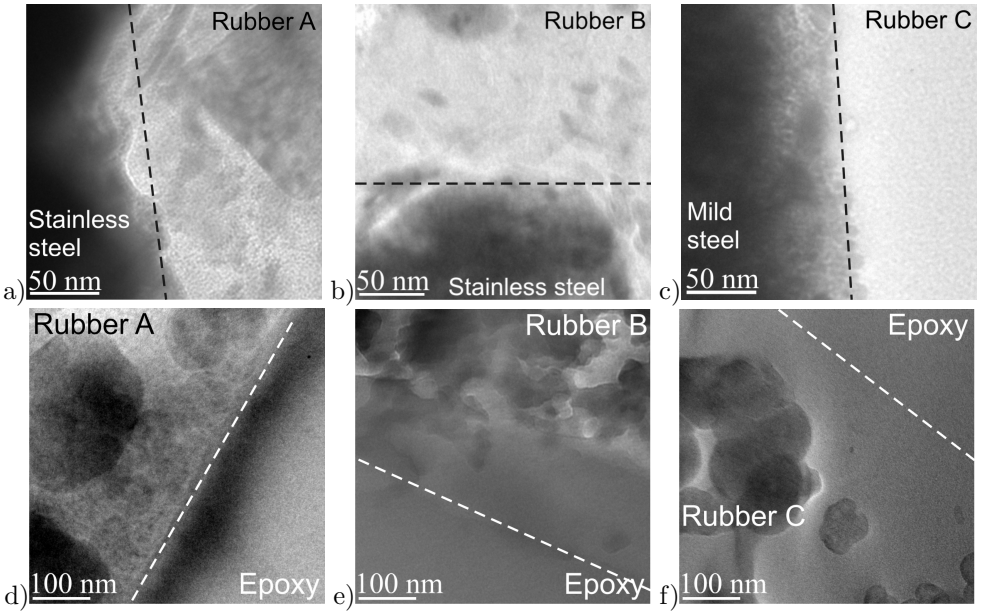

Figure 6.3: *Cross-sectional TEM images from the substrate/rubber interfaces. Note the different scale bars in figures (a-c) and (d-f). [Publication I]*

6.2 Adhesion studies and environmental testing

The peel test results

The peel tests were begun with the non-exposed mild steel/rubber C specimens. However, in all test samples the rubber broke cohesively before the peeling was started (see Figs. 6.4a and 6.5a) and thus the peel strength for the interface could not be determined. This clearly indicates that the cohesive strength of rubber C is less than its peel strength when attached to the mild steel. Similar to the non-exposed samples, the isothermal and the isohume exposed mild steel/rubber C samples exhibited cohesive fracture. The peel force at which the non-exposed rubber C fractured was around 70 N and it remained at the same level after the exposure to hot or moist environments. However, hygrothermal ageing lead to adhesive fracture (similar to Figs. 6.4b and 6.5b) together with a distinct decrease in the peel force. The peel test results are summarized in Table 6.2. Since mild steel/rubber combinations are widely used in industrial applications, such as in vibration damping devices [83], the mild steel/rubber C results were set as a point of comparison to the corresponding stainless steel hybrids. The composite/rubber C samples showed only cohesive fracture before and after ageing.

For the stainless steel surfaces, rubber B was studied first. At the non-exposed stage, all samples showed adhesive fracture. The adhesion of the 2J/rubber B and IP/rubber B interfaces was negligible and the peel strength determination was not possible. Thus, the 2J and IP surfaces were not studied further at all. The rough SB surface showed the highest peel strength, as shown in Table 6.2. Within quite similar 2B and 2D surfaces, the 2D surface was chosen over 2B for further studies due to its higher peel strength. The ageing of the stainless steel/rubber B samples decreased the peel forces (Table 6.2) except for the SB/rubber B samples which fractured cohesively after isothermal ageing. The fracture of rubber B from composite substrate was otherwise cohesive but after hygrothermal ageing adhesive fracture was observed. The peel force, at which rubber B fractured cohesively, decreased from 268 N (non-exposed) to around 55 N due to ageing (hot or moist exposure). During the peel tests of the composite surface and the stainless steel surfaces 2B, 2D and SB, it was observed that rather than following the peel test roller and a peel angle of 45°, the rubber strip tended to show a higher peel angle.

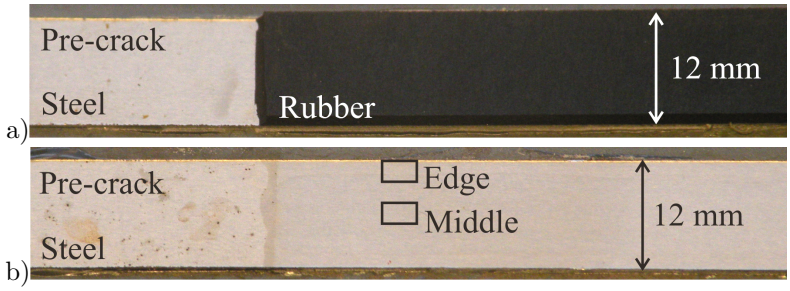

Figure 6.4: *Top view photographs of (a) a cohesively fractured sample and (b) an adhesively fractured sample. The pre crack and the studied middle and edge areas are also shown. [Publication II]*

Table 6.2: *A summary of the floating roller peel test results. The peel strength was not possible to be determined for the samples in which the peel strength exceeded the rubber's cohesive strength (referred as "cohesive"). [Combination from publications I and II, including also some unpublished data].*

Sample			Interfacial Peel Strength [N/mm]			
Substrate	**Surface**	**Rubber**	**Non-exposed**	**Iso-thermal**	**Isohume**	**Hygro-thermal**
Stainless steel	*2D*	*A*	*Cohesive*	*Cohesive*	*Cohesive*	*Cohesive*
	SB	*A*	*Cohesive*	*Cohesive*	*Cohesive*	*Cohesive*
Stainless steel	*2D*	*B*	*0.90±0.08*	*0.87±0.16*	*0.70±0.12*	*0.21±0.03*
	SB	*B*	*26.88±1.44*	*Cohesive*	*2.99±0.16*	*1.52±0.13*
	2B	*B*	*0.74±0.19*	*0.48±0.07*	*0.32±0.11*	*0.47±0.14*
	2J	*B*	-	-	-	-
	IP	*B*	-	-	-	-
Mild steel	*CR*	*C*	*Cohesive*	*Cohesive*	*Cohesive*	*0.66±0.33*
GFRP	*Peel ply*	*A*	*Cohesive*	*Cohesive*	*Cohesive*	*Cohesive*
	Peel ply	*B*	*Cohesive*	*Cohesive*	*Cohesive*	*2.60±0.14*
	Peel ply	*C*	*Cohesive*	*Cohesive*	*Cohesive*	*Cohesive*

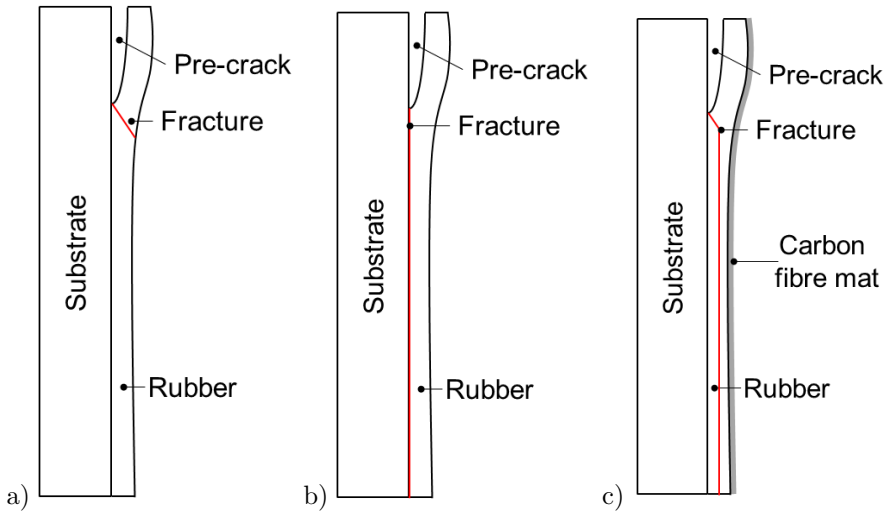

Figure 6.5: *Schematic presentations of the fracture location in (a) cohesively fractured samples, (b) adhesively fractured samples and (c)carbon fibre mat reinforced samples.*

Rubber A fractured cohesively from all studied substrates, namely from stainless steel 2D and SB and composite surfaces, before and after all ageing procedures. Thus rubber A showed the best behaviour within the studied rubber grades. For the non-exposed samples the peel force, at which the rubber failed, was around 382 N but the force decreased to 42-45 N for the exposed samples.

In order to verify that the cohesively fractured rubber/substrate interfaces were really stronger than the rubbers, a new set of samples was prepared. In these specimens, a flexible carbon fibre mat was added to the rubber's outer surface before vulcanisation to prevent the fracture of rubber. However, in all these samples the failure locus was still inside the rubber, as shown in Fig. 6.5c.

The adhesively fractured peel test samples were studied with SEM and due to the better adhesion properties of rubbers A and C, for which adhesively fractured surfaces were not comprehensively available, the studies were concentrated on rubber B samples. The stainless steel surfaces showed partial adhesive/cohesive fracture (Fig. 6.6). In the sand blasted surface, the rubber B residues were distributed quite uniformly to the asperities of the surface (Fig. 6.6a) whereas on the 2B and 2D surfaces the cohesive fracture was found mainly from the grain boundaries as shown in Fig. 6.6b. However, some rubber residues were found also on the smooth areas of the surfaces. The isothermally aged samples showed higher amount of rubber residues on the steel surface than the other 2B and 2D surfaces (Fig. 6.6c). This implies that thermal ageing has an improving effect on the strength of the stainless steel/rubber B interface. No remarkable difference was observed between the non-exposed samples and those exposed in isohume environments, as can be seen in Fig. 6.6d. The steel substrates of the hygrothermally aged samples showed less rubber residues, i.e. less cohesive fracture, after adhesive fracture in the edge areas of the peel test samples than in the middle areas (Fig. 6.6e-f, see also Fig. 6.4). The degraded, less tightly bound area was roughly 2 mm wide at the both sides of the 12 mm wide samples. Similar behaviour was found in the hygrothermally aged composite/rubber B and mild steel/rubber C samples.

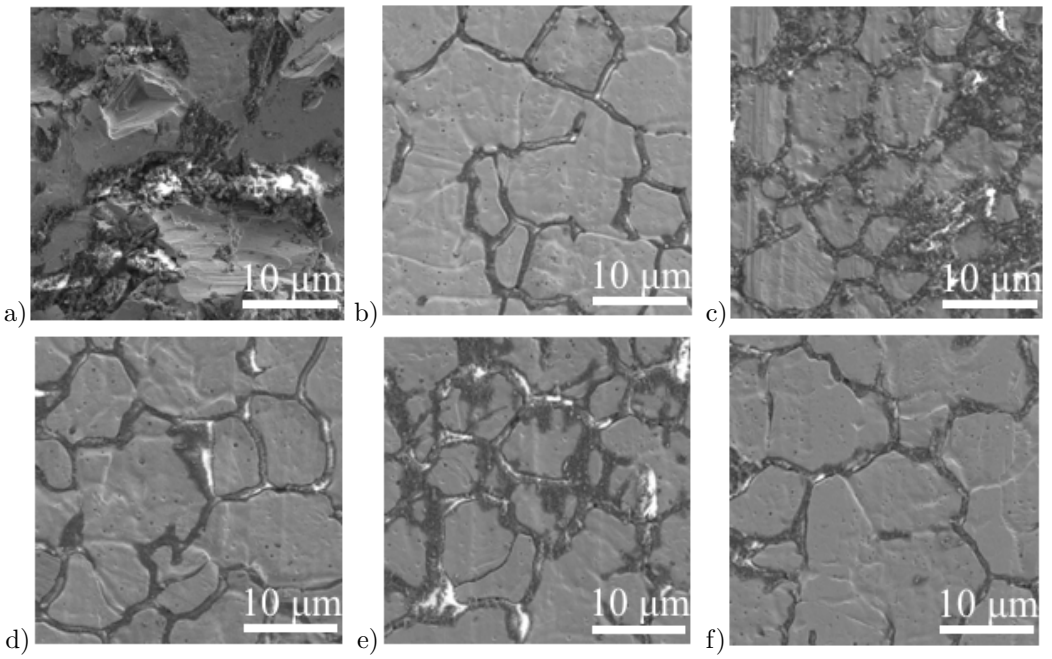

Figure 6.6: *The peeled stainless steel/rubber B substrates: (a) non-exposed SB surface, (b) non-exposed 2D surface, (c) isothermally aged 2D surface and (d) isohume exposed 2D surface. The hygrothermally exposed 2D surface is shown in (e) from the middle area and in (f) from the edge area of the sample. [Publication II]*

Changes in rubbers due to the ageing

The possible changes of the rubbers before and after hygrothermal ageing of the adhesively fractured rubber B were studied by FT-IR. Other rubber grades did not allow studies of the peeled rubber surface due to the cohesive fracture. The spectra for the non-exposed and for the hygrothermally exposed stainless steel 2D/rubber B samples were similar, as can be seen from Fig. 6.7. However, there was a small difference at the area of hydrogen bonded OH groups (3200-3600 cm^{-1} [84]) shown in the insert A of Fig. 6.7. This suggests that the fraction of hydrogen bonded water has increased during the exposure in the interface and it remains on the interfacial area also after 72 hours stabilisation at 23 °C and 50%RH. However, the change is minor. Although no chemical changes in the polymer structure were observed, the absorbed water may have decreased the peel strengths through plasticisation effects [85].

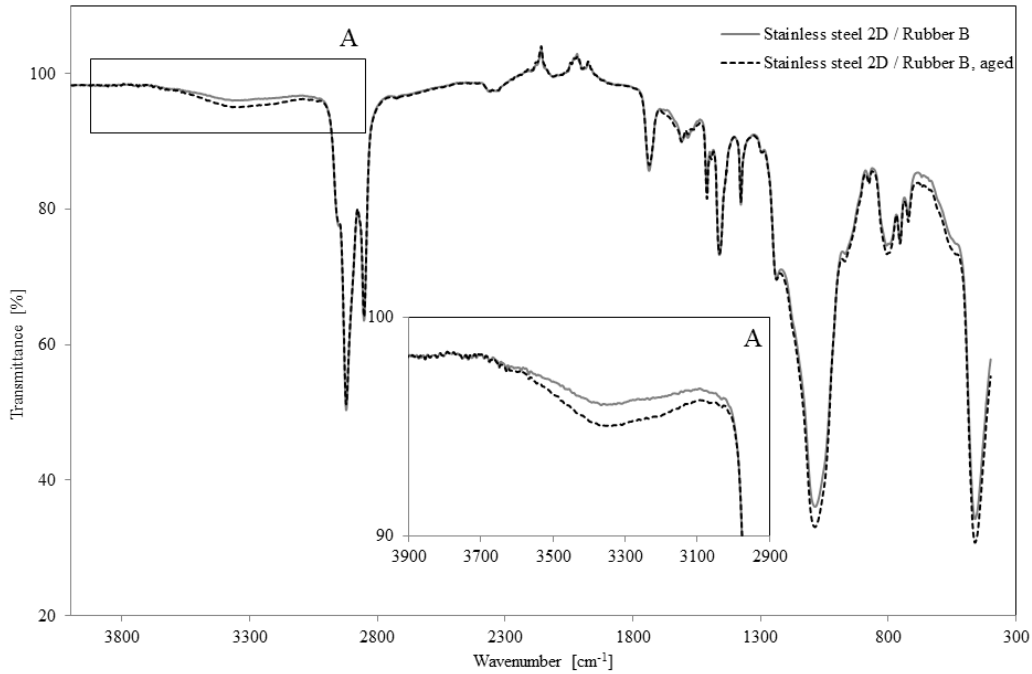

Figure 6.7: *The FT-IR spectra of non-exposed and hygrothermally aged rubber B peeled from the stainless steel surface 2D. The spectrum of the aged rubber is measured from the edge area of the sample (see Fig. 6.4). [Publication II]*

The possible changes in the different rubber grades due to the hygrothermal exposure were also studied by TGA and the results are shown in Fig. 6.8. The aged rubber grade A did not show changes due to the ageing, whereas minor degradation of the aged B and C samples was observed in the form of a small shift in the main steps (400-500 °C) of the TGA curves. In rubber B, the degradation of the aged sample begins a little earlier when compared to

the non-exposed sample. However, the temperature, at which the degradation takes place, and the amount of inert residue remain unaltered. The degradation of the aged rubber C is delayed slightly, the degradation temperature is increased and the apparent elastomer fraction is decreased more significantly than for the other rubber grades (15% vs. 8%). These changes may indicate an increase in cross-link density due to hygrothermal exposure. All in all, the changes in rubber B and C are minor.

The Shore D hardness before ageing for rubbers A, B, and C was 41 ± 1.2, 43 ± 0.9, and 44 ± 0.8, respectively. Changes in hardness due to hot, moist or hot/moist environment were not observed for rubbers A and B as the Shore D values stayed within the standard deviation limits. A slight increase in hardness was observed for rubber C (47 ± 0.9 after hygrothermal ageing). This supports the assumption that hygrothermal exposure has caused an increase in the cross-link density of rubber C.

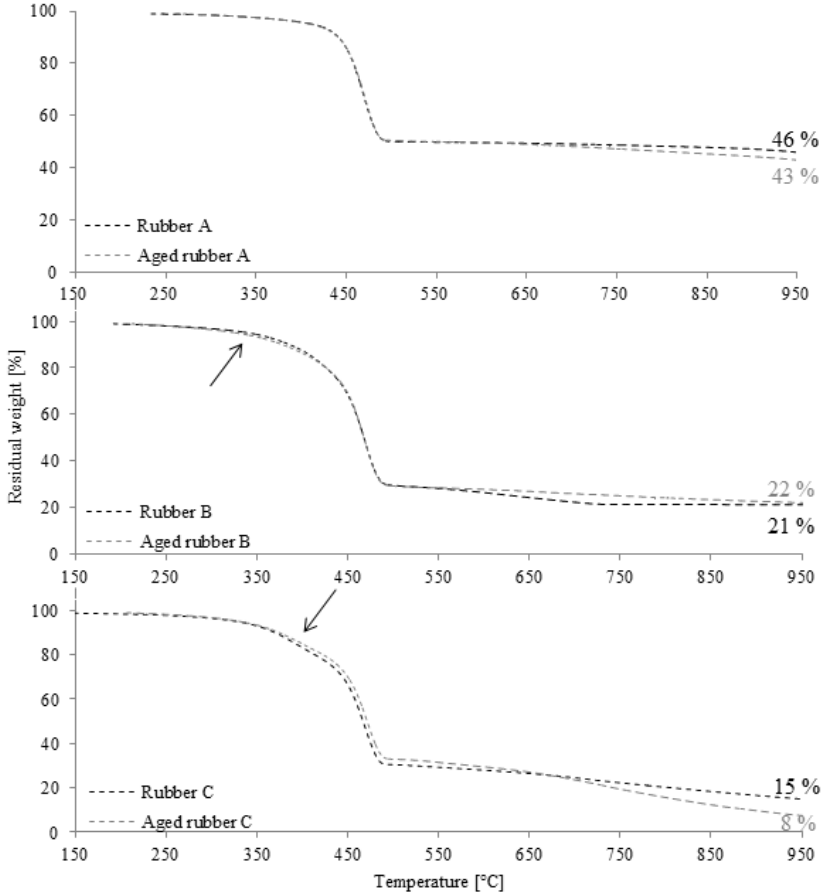

Figure 6.8: *The thermogravimetric spectra of the non-exposed and hygrothermally exposed rubbers A-C. The curves are plotted starting from the point where the mass has decreased one percentage unit (weight 99%). In addition, the weight of the inert residue is reported. Modified from [Publication II].*

The SCB test results

The SCB tests were started with the mild steel/rubber C/composite samples having the pre-crack between the steel and the rubber. However, during these tests the crack always deflected to the composite/rubber interface and the interfacial fracture energy of the steel/rubber interface could not be determined. In the samples where the pre-crack was in the composite/rubber interface and the rubber thickness was 1.6 mm, directionally unstable cracks and crack propagation in both interfaces were observed and thus the results were not reliable. Therefore, the interfacial fracture energies were measured only for the rubber thicknesses of 0.5 mm and 0.7 mm. The cross head rate dependence was studied with rubber thickness of 0.7 mm

The samples showed initial linear force-displacement behaviour until the maximum load was achieved. The maximum load depended on the rubber thickness and the cross head rate. Similar dependency has been found for thermoplastic/steel hybrids [15]. The interfacial fracture energy results are shown in Fig. 6.9. Thicker rubber led to lower interfacial fracture energy values while the interfacial fracture energy increased with increasing cross head rate.

6.3 Vibration damping test results

The FRF_{mean} curves were calculated for all specimens from the vibration damping test data. A shift of certain resonance frequencies towards higher frequencies was seen in the samples with thicker rubber layer as shown in Fig. 6.10. The loss factor results are shown for the plain steel plates and for the composite plate in Fig. 6.11 and the DMA result for the rubbers in Fig. 6.12.

The rule of mixtures (ROM) was employed for the hybrids' results to investigate if the ROM method would be applicable for this kind of structures. The results for the plain steel and composite sheets and the DMA results for the rubbers were used as starting values. It was assumed, that the saturation of the DMA results of the rubber grades would stay at a constant loss factor level until 500 Hz. Both weight fractions and volume fractions were used to weight the individual components' loss factor values. The ROM results for the steel/rubber/composite hybrids are depicted together with the experimental data in Figs. 6.13 and 6.14. The root-mean-square deviation (RMSD) values for the weight and the volume fraction ROM estimations and their comparison to the experimental data are shown in Table 6.3.

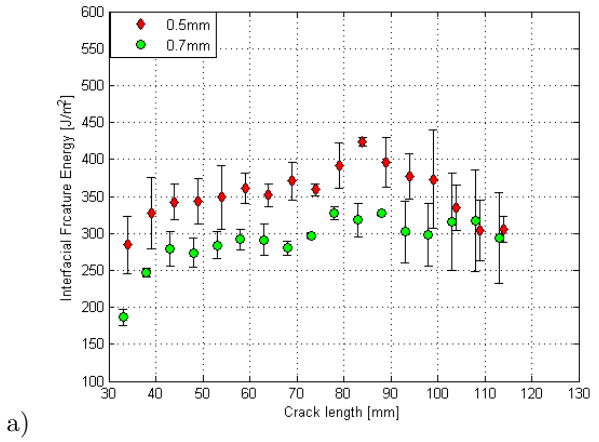

a)

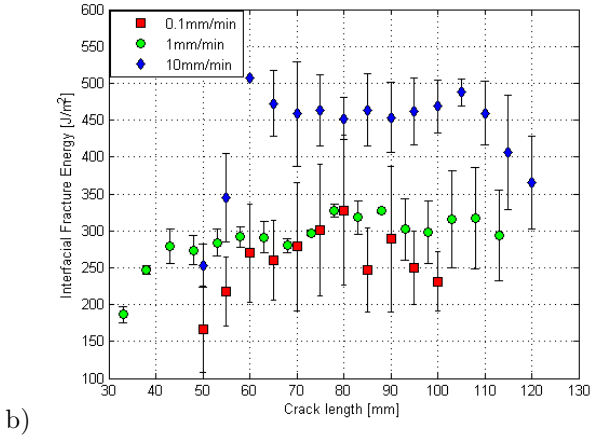

b)

Figure 6.9: *The interfacial fracture energy results for composite/rubber C interface: (a) for two different rubber thicknesses at the load rate of 1.0 mm/min and (b) for three different load rates at the rubber thickness of 0.7 mm [Publication III].*

Table 6.3: *The root-mean-square deviation (RMSD) values for the weight and the volume fraction ROM estimations when compared with the experimental data for the mild steel and stainless steel based hybrids. Modified from [Publication IV].*

	Sample		**RMSD for weight fraction ROM estimation**	**RMSD for volume fraction ROM estimation**
Mild steel	*Rubber C 0.5 mm*	*GFRP*	*0.0087*	*0.0132*
	Rubber C 1.0 mm		*0.0120*	*0.0186*
	Rubber C 1.5 mm		*0.0089*	*0.0198*
Stainless steel	*Rubber B 0.5 mm*	*GFRP*	*0.0110*	*0.0180*
	Rubber B 1.0 mm		*0.0092*	*0.0148*
	Rubber B 1.5 mm		*0.0066*	*0.0134*

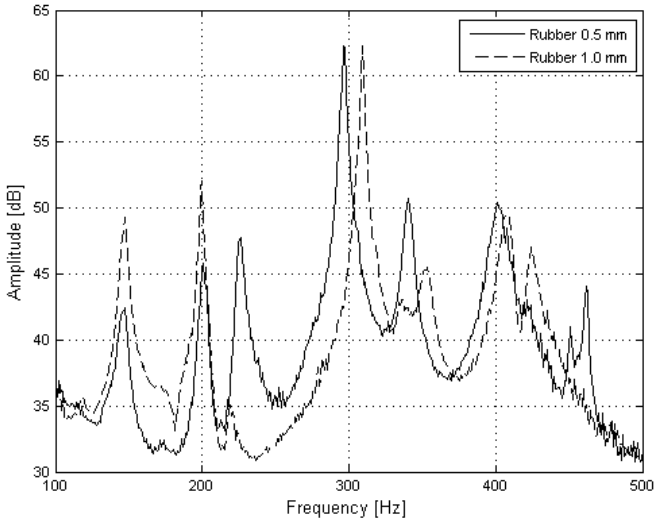

Figure 6.10: *Examples of the average response curves of the frequency domain tests for the stainless steel/rubber B/composite hybrids [Publication IV].*

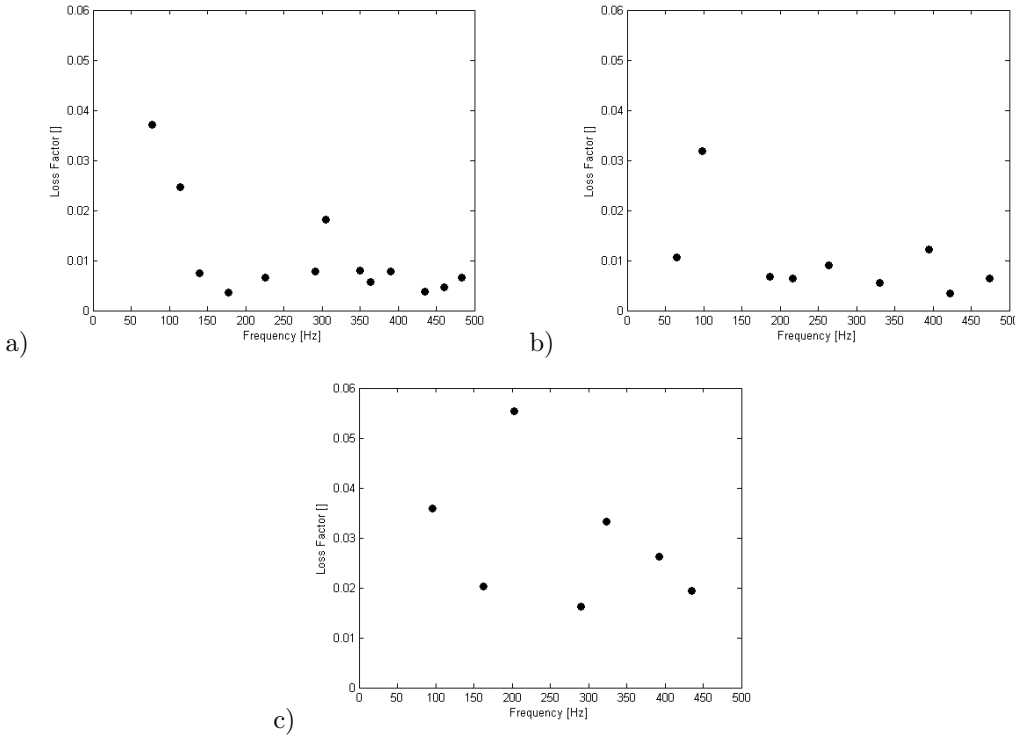

Figure 6.11: *The loss factor results for (a) mild steel, (b) stainless steel and (c) composite plates [Publication IV].*

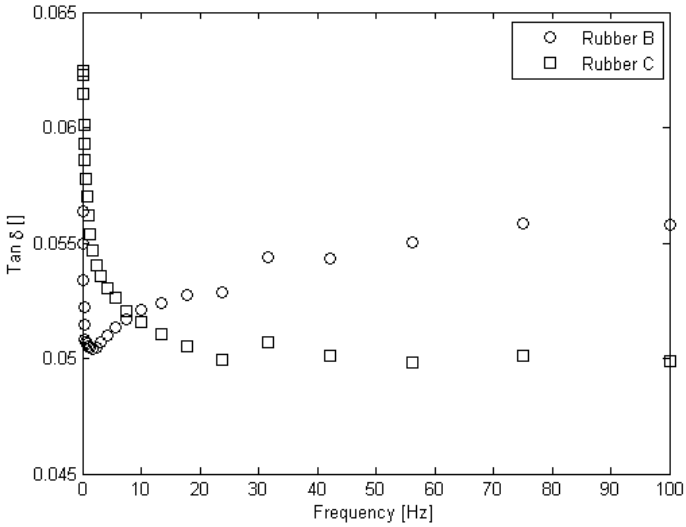

Figure 6.12: *The DMA results for rubbers B and C [Publication IV].*

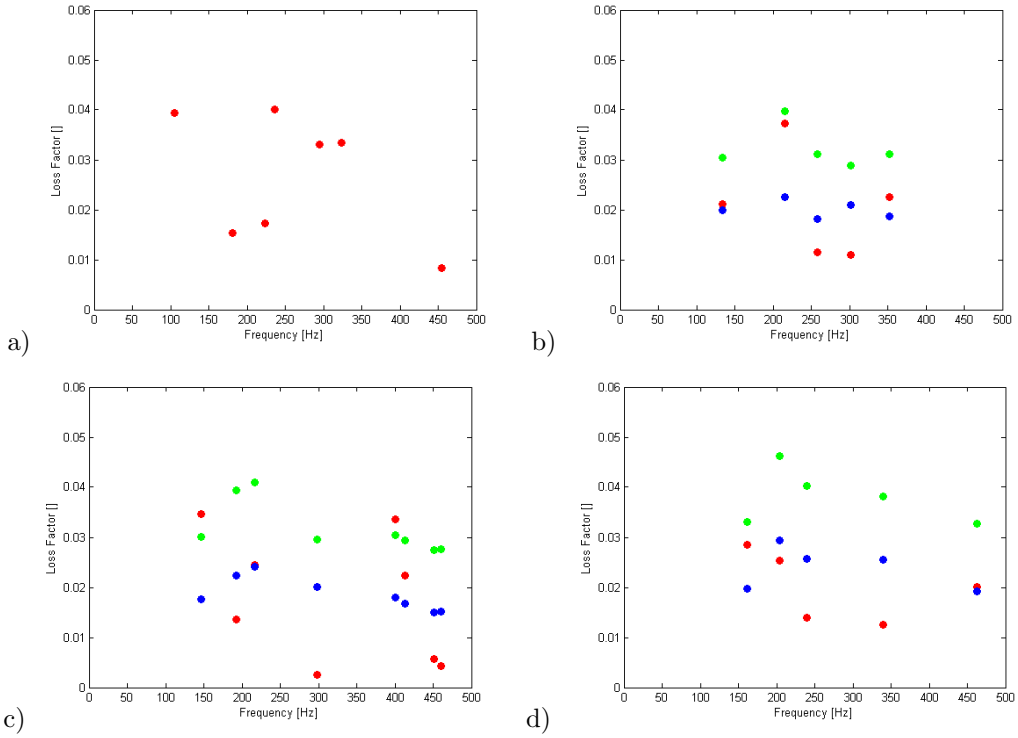

Figure 6.13: *The frequency domain test results (red), the weight fraction ROM results (blue), and the volume fraction ROM results (green) for mild steel based hybrids: (a)with epoxy adhesive and with rubber C thickness of (b) 0.5 mm, (c) 1.0 mm and (d) 1.5 mm [Publication IV].*

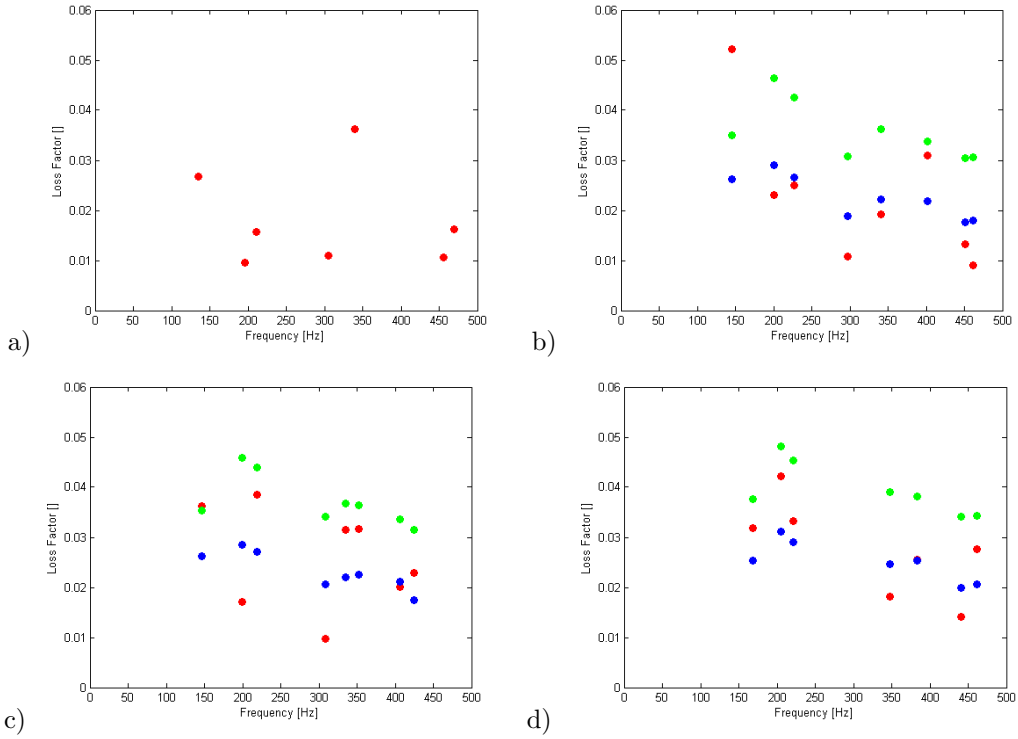

Figure 6.14: *The frequency domain test results (red), the weight fraction ROM results (blue), and the volume fraction ROM results (green) for stainless steel based hybrids: (a)with epoxy adhesive and with rubber B thickness of (b) 0.5 mm, (c) 1.0 mm and (d) 1.5 mm [Publication IV].*

6.4 Impact test results

In general, the high velocity impacts caused plastic deformation to the steel sheet and different types of damages of the composite sheet (Fig. 6.15). The shape of the impact crater in the steel surface was droplet like due to the impact angle less than 90°. At higher impact energies the composite damage area exceeded the impact crater area of the steel sheet, as in Fig. 6.15. The damage size of the composite layer was described by damage area (Fig. 6.15c). The non-transparent area of the composite sheet was considered as damaged area.

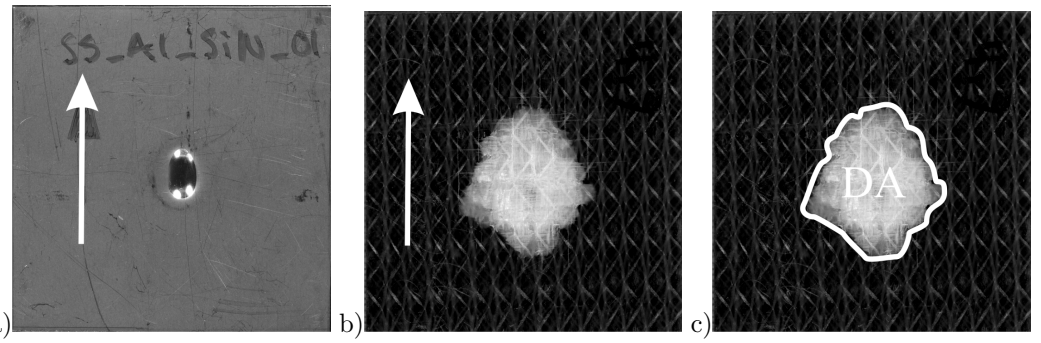

Figure 6.15: *Impact tested stainless steel/rubber A/composite hybrid sample (a) from the steel and (b) from the composite side. The damage area (DA) is shown in (c). The arrows show the direction of the impact. [Publication V]*

The impact test results are shown in Figs. 6.16-6.21. The Fig. 6.16a shows that the inclusion of rubber instead of epoxy decreased the damage area by 26-47% for the stainless steel based hybrids (rubbers A and B) and 4-23% for the mild steel based hybrids (rubber C), depending on the rubber thickness. However, within rubber grades A and C, the increase in the rubber thickness from 0.5 to 1.5 mm did not decrease the damage size remarkably but it rather stayed within the standard deviation limits. Only rubber B shows decreasing trend in damage area with increasing rubber thickness. On the contrary to the damage area, the dissipated energy (Fig. 6.16b) did not seem to depend on the existence or thickness of the rubber layer. The absorbed energy values are expressed as percentages of the original impact energy of 15 joules.

At the studied energy range, the damage area showed linear behaviour with increasing impact energy whereas it was accompanied by only a slight increase in absorbed energy (Fig. 6.17). An increase in the dissipated energy and in the damage area was observed with increasing impact angle (Fig. 6.18). Increasing projectile velocity induced a slight increase from 72% to 80% in the absorbed energy together with an increase of 21% in the damage area (Fig. 6.19). The temperature dependency of the steel/rubber/composite hybrid was marginal in the case of damage area and absorbed energy (from 34.8 $\pm$ 6.6 mm^2 to 40.0 $\pm$ 1.5 mm^2 and from 71.6 $\pm$ 1.5% to 81.0 $\pm$ 0.8%), as shown in Fig. 6.20. Also differences between the non-exposed samples (damage area 37.7 $\pm$ 2.4 mm^2 and energy absorbed 76.9 $\pm$ 1.8%) and the aged samples (damage area 32.7 $\pm$ 3.0 mm^2 and energy absorbed 78.5 $\pm$ 2.6%) were minimal.

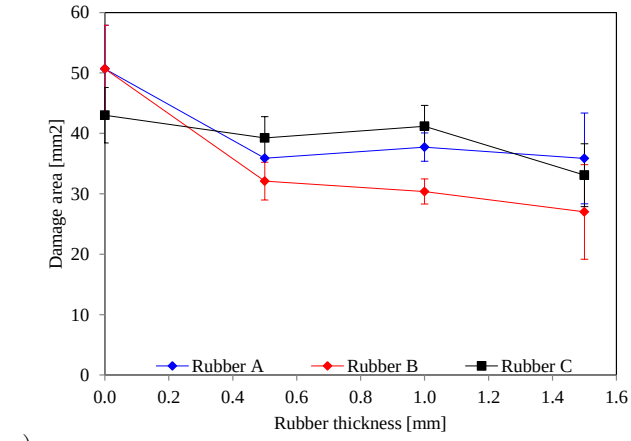

a)

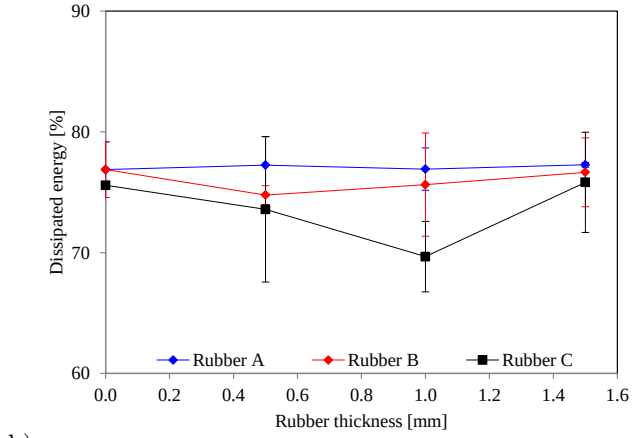

b)

Figure 6.16: *Damage area versus rubber thickness is shown in (a) and dissipated energy versus rubber thickness in (b) for different steel/rubber/composite hybrids [Publication V].*

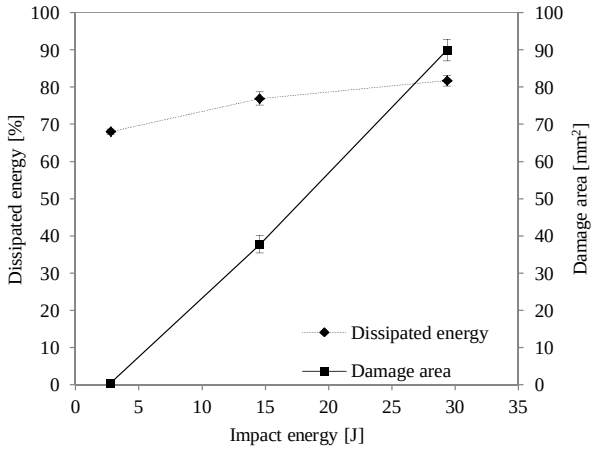

Figure 6.17: *Damage area and dissipated energy versus impact energy for stainless steel/rubber A/composite hybrid [Publication V].*

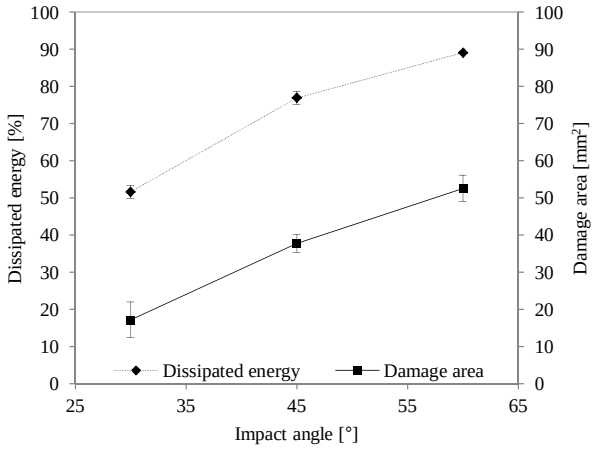

Figure 6.18: *Damage area and dissipated energy versus impact angle for stainless steel/rubber A/composite hybrid.*

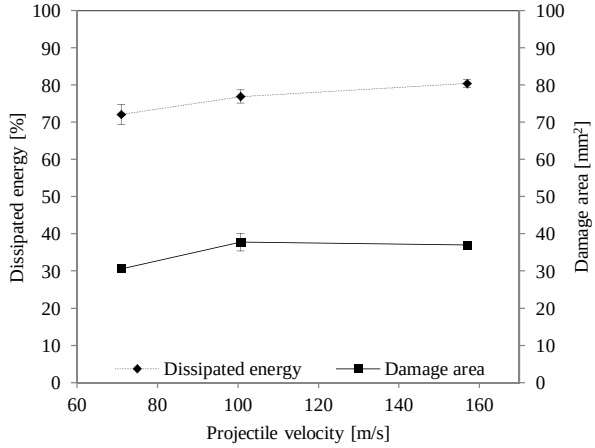

Figure 6.19: *Damage area and dissipated energy versus projectile velocity for stainless steel/rubber A/composite hybrid.*

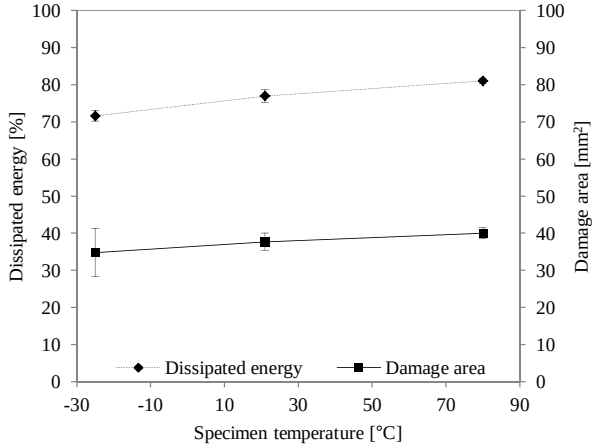

Figure 6.20: *Damage area and dissipated energy versus specimen temperature for stainless steel/rubber A/composite hybrid.*

The damage area in the samples impacted with 3 joules ten times increased gradually with increasing number of impacts (Fig. 6.21a). For the stainless steel/rubber A/composite hybrids the increase of the composite damage area intensified with subsequent impacts, whereas in the epoxy based hybrids the composite damage area seemed to stabilise. The stabilisation was accompanied by composite/epoxy adhesive delamination, which was observed after the second or third impact. The delaminated area grew much faster than the composite damage area and exceeded the free sample area (diameter 40 mm) after fourth or fifth impact (Fig. 6.22). In the stainless steel/rubber A/composite hybrid structures delamination was not observed. However, after the first impact, line-like defects appeared in the composite layer (visible in Fig. 6.22a). Still, the composite damage area was determined according to the non-transparent composite area instead of the maximum damage diameter of the line defects. The dissipated energy was slightly lower for the epoxy adhesive based hybrids and stayed approximately within the standard deviation values for the both hybrid types (Fig. 6.21b).

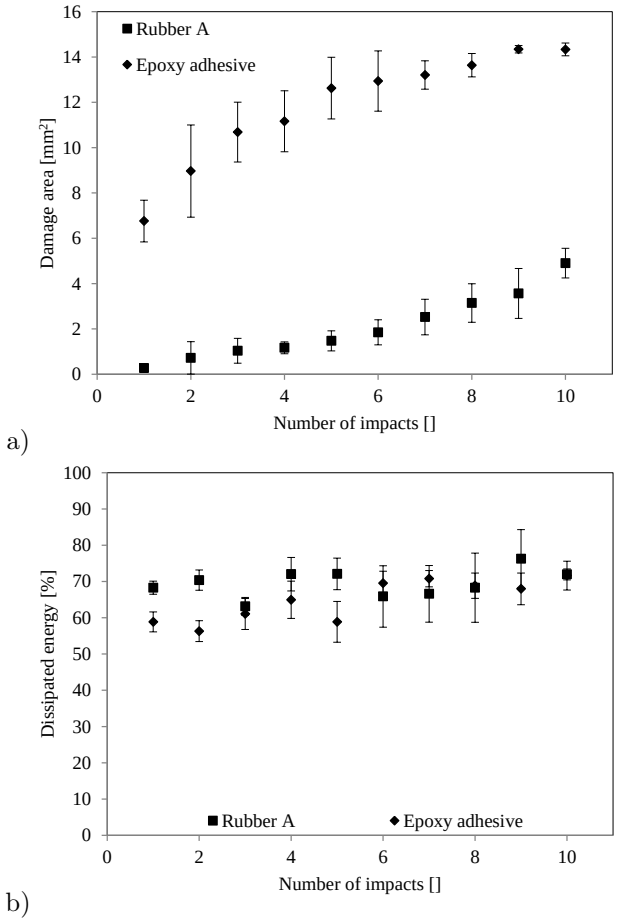

Figure 6.21: *Figure (a) shows damage area and (b) dissipated energy versus the number of impacts for stainless steel/rubber A/composite and stainless steel/epoxy adhesive/composite hybrid structures.*

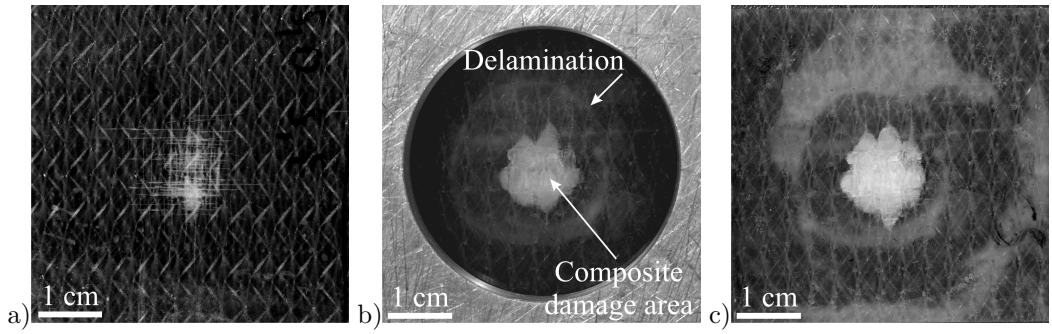

Figure 6.22: *Photographs of (a) stainless steel/rubber A/composite hybrid structure after 10 impacts (á 3 J), (b) stainless steel/epoxy adhesive/composite hybrid structure after 3 impacts (á 3 J), and (c) stainless steel/epoxy adhesive/composite hybrid structure after 10 impacts (á 3 J).*

From the cross-sectional SEM images of the impact test samples, it was possible to evaluate the dimensions (length and depth) of the impact craters. Generally, the crater length decreased with increasing rubber thickness, although in the mild steel/rubber C/composite hybrids an increase in the crater length with the thickest rubber layer was observed. In addition, the crater depth increased with increasing rubber thickness for all samples. A clear increase in impact crater dimensions was found with increasing impact energy and impact angle. The other test parameters did not show any clear trend in the impact crater dimensions excluding the effect of temperature: the impact crater depth increased from 0.7 mm to 1.1 mm with the increase of 105 °C in temperature. Also, the depth of the impact craters increased with repeated impacts. In general, the crater dimensions in the mild steel based samples were smaller than in the stainless steel based samples.

According to the cross-sectional SEM studies, the primary damage mechanisms of the steel/rubber/composite hybrids were interfacial delamination and fibre/matrix debonding (Fig. 6.23). In addition, fibre breakage and matrix cracks were found to a minor extent. In general, the most clearly delaminated parts were concentrated in the areas where the plastic deformation of the steel was strongest, as shown schematically in Fig. 6.24. The central areas of the impact craters had typically a tight contact between the components. No steel/rubber delaminations were found and only a few delaminated stretches of composite/rubber interface were found at the central areas of the impact craters. Outside the impact crater, the delaminated areas did not appear to be continuous throughout the delamination width in either of the interfaces. However, when observing and analysing delamination by SEM, it should be kept in mind that cutting and grinding, as a part of the sample preparation process, may cause changes in the delamination dimensions at the sample surface. Delamination can be extended by peeling the components apart or decreased by smearing the rubber over the other component. Thus, the delaminations cannot be reliably determined by SEM. The visual inspection of the delamination in the composite/rubber interface is possible due to the transparency of the composite sheet and the interfacial delamination was not observed to exceed the damaged area of the composite, which is opaque. In the samples without rubber, delaminations in the steel/epoxy interfaces were found, whereas the composite/epoxy interfaces were intact. However, no clear difference in the composite damage density was found when compared with the rubber bonded samples.

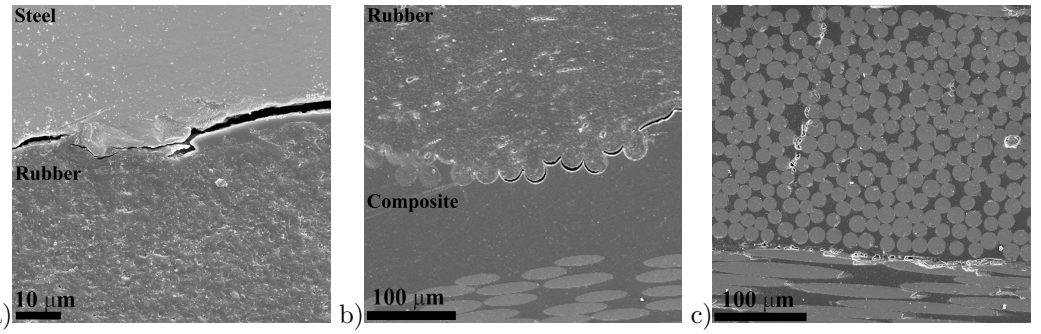

Figure 6.23: *The main damage mechanisms: (a) steel/rubber delamination (b) composite/rubber delamination and (c) fibre/matrix debonding [Publication V].*

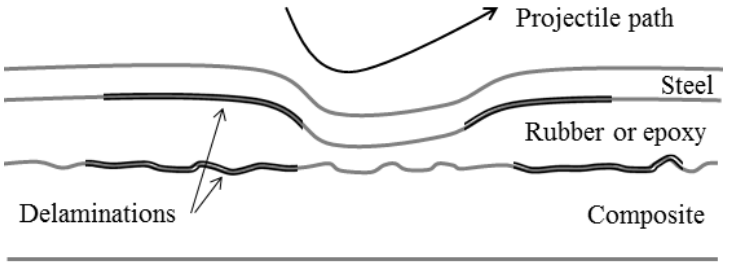

Figure 6.24: *Schematic presentation of the typical locations of the delaminations. Modified from [Publication V].*

Increasing impact energy caused higher damage density in the composite (Fig. 6.25). Although Fig. 6.19 shows clearest difference in damage area and in dissipated energy between the projectile velocities of 71 m/s (WC ball) and 100 m/s (steel ball), the highest velocity of 157 m/s (Si_3N_4 ball) caused clearly highest damage density into the composite layer. Damages in the samples impacted with the highest velocity were concentrated on the back side of the sample whereas the damage density close to the composite/rubber interface was smaller. Also higher impact angle caused higher composite damage density and the damages were concentrated again on the back side of the sample. The differences between the impact angles of 30° and 45° were smaller than between the impact angles of 45° and 60°.

The main damage mechanisms did not show any difference between the samples loaded at different temperatures. Some rubber fractures in the composite/rubber interface of the hot samples was found, which was unique for these test parameters. No differences were found in the cross-sectional SEM images of the aged samples when compared with the non-exposed ones.

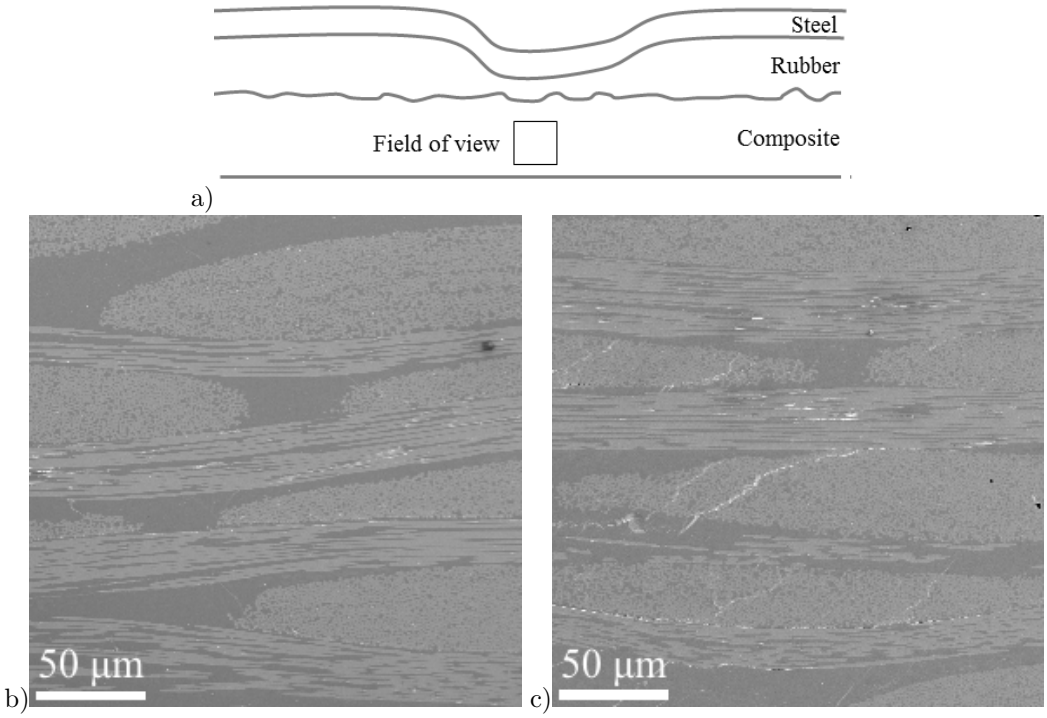

Figure 6.25: *A shematic presentation of the field of fiew is shown in (a) and composite damage in specimens impacted with a projectile velocity of (a) 71 m/s and (b) 157 m/s.*

7 Discussion

In this chapter, the results described in the previous chapter are discussed. The chapter is divided in two subsections: the first part concentrates on the adhesion properties of the studied steel/rubber/composite structure discussing the cross-section microscopy and adhesion test results. The second part concentrates on the energy absorption properties discussing the vibration damping and high velocity impact test results.

7.1 Adhesion properties of the steel/rubber/composite hybrid structures

The absence of discontinuities in any of the substrate/rubber interfaces in the cross-sectional scanning electron microscopy (SEM) or in the more detailed cross-sectional transmission electron microscopy (TEM) images indicates that the manufacturing method creates high quality interfaces between the substrates and the rubbers. Figs. 6.6b-f imply that mechanical interlocking of rubber into the grain boundaries is the main reason for higher peel strengths of rougher stainless steel surfaces. Similarly, the rough sand blasted surface (Fig. 6.1d) has enabled significant mechanical interlocking of rubber (Fig. 6.6a).

Within the studied rubber grades, rubber A showed the best adhesion properties, even better than rubber C to mild steel. Since the substrate/rubber A samples fractured always cohesively inside the rubber, no differences between the substrates were observed. In addition, ageing did not change the location of the fracture but the rubbers fractured cohesively. Thus it can be concluded that by choosing suitable rubber composition, neither time-consuming pre-treatments, nor adhesives are needed to create a well-bonded stainless steel/composite hybrid structure using a thin rubber layer. Consequently the use of rubber simplifies the hybrid's manufacturing process substantially when compared to the conventional adhesion methods. In addition, it can be assumed that the strength of the structure exceeds the cohesive strength of the rubber and the reliability of the structure can be estimated with the knowledge of the rubber's bulk properties.

Rubber A exhibited very good adhesion properties whereas the adhesion of rubber B to the substrates was not as good as the adhesion of rubber C to mild steel. However, the adhesive fracture of rubber B from the stainless steel substrates enabled the investigation of the effect of the substrate surface roughness. As expected, the rough sand blasted stainless steel surface and the peel ply treated composite surface exhibited superior peel strength when compared with the industrial surface finishes, whereas the adhesion level of rubber B to the polished surface was negligible. Within the industrial surface finishes, the 2D surface (cold rolled, heat treated, pickled) provided slightly better adhesion, which can be explained by the rougher surface (higher R_a value, Table 6.1) of 2D when compared with 2B surface (cold rolled, heat treated, pickled, skin passed). The negligible adhesion between rubber B and the brushed stainless steel surface 2J is supposed to be due to the lack of strong mechanical interlocking, which is not provided by the oriented grooves of the 2J surface. Fig. 7.1 shows that there is a clear dependency between the surface roughness and the peel strength. This

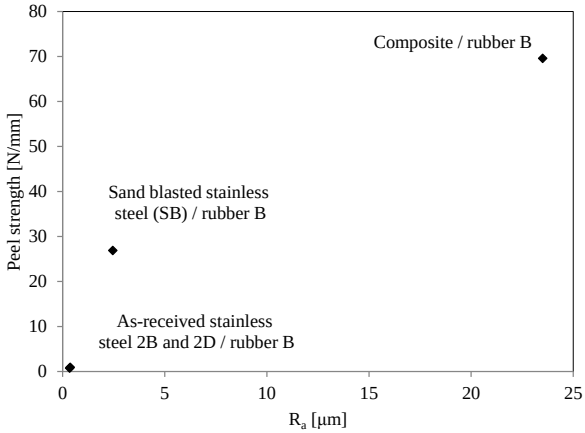

Figure 7.1: *Peel strength of rubber B versus the R_a value of the substrate. Derived from the results of [Publication I].*

together with the SEM results imply that the adhesion of rubber B to substrates arises mainly from mechanical interlocking. Whether the dependency between the surface roughness and peel strength is linear or not, it is impossible to say due to the small number of the measurement points in Fig. 7.1. However, according to the SEM studies, there were some rubber residues on the smooth areas outside the grain boundaries on the peeled 2D surface and on the smoother 2J and IP surfaces. This suggests that chemical adhesion mechanisms are present as well.Further, these adhesion mechanisms are probably substrate-dependent.

Ageing affected the rubber B adhesion. While exposure to isohume environment had only a small effect, the increased amount of rubber residues on the 2B and 2D surfaces and the change of the fracture mode from adhesive (interfacial) to cohesive (inside the rubber) on the SB surface after the isothermal ageing would indicate that elevated temperatures enhance the interfacial strength of the stainless steel/rubber B structure. However, an increase in the peel strength was not observed in the other stainless steel/rubber B samples after isothermal ageing. The peel test results of the hygrothermally aged samples showed that stainless steel/rubber B and composite/rubber B joints are not environmentally resistant. Based on the results of the Fourier transform infrared (FT-IR), thermogravimetric analysis (TGA) and Shore D hardness measurements, significant changes in the rubbers were not observed. Typically, the adhesion mechanism between organic and inorganic surfaces (i.e between metal and polymer) is thought to be electrostatic adhesion [86], which is prone to humidity [41]. For example, Ozawa *et al.* have shown that increased temperature and humidity lead to increased oxygen content in a brass/natural rubber (NR) interface [87]. Their assumption is that in humid environment, water decomposes upon infiltration into rubber increasing the oxygen density in the rubber and in the brass/rubber interface which promotes such changes in the oxide structure of the brass surface that weaken the interfacial adhesion strength [87]. Ethylene propylene diene terpolymer (EPDM) based rubbers are typically impermeable to water and they are used widely in different sealing applications [73], although the permeability coefficient values of EPDM rubbers vary remarkably up to the values reported for natural rubber depending on the exact composition of the rubber [88, 89]. Thus, it can be assumed that the infiltration of water through the rubber

is minimal but the infiltration of humidity may have taken place along the interface. This is supported by the observation that rubber has been less tightly bound to the steel at the edge of the peel test sample than in the middle areas. Deductions about the changes or the interface at molecular level are not possible to be done since the exact composition of the rubbers are not available and thus the detailed mechanisms of the chemical changes in the stainless steel/rubber interface in hot/moist environment should be studied further. Those results could be utilized to develop more reliable stainless steel/rubber components.

The adhesion level of the interface is determined by the micro and the macro nature of the substrate surface and the mechanical and the physical properties of the adherends [90]. However, the peel test results depend also on the test geometry and the environment. The test parameters affecting the measured peel strength are peel angle, peeled film thickness, peeling rate, the material properties of the substrate and the film, and the environment, in which the peel test is performed [75]. Thus it is difficult to compare one peel test results to others. In this study the results of rubber C, which acts as a reference material, are rather thought as qualitative in nature: the cohesive fracture of rubber in all samples except the hygrothermally aged mild steel/rubber C specimens is thought to be the reference level. Thus, rubber A is found to rise above the reference structure. In addition, rubber A at all studied substrates and rubber B on the sand blasted stainless steel surface exceeded clearly the peel strength values of a non-aged mild steel/natural rubber interface (peel angle 45°) [74] and stainless steel/thermoplastic urethane interface (peel angle 180°) [91] found in literature. The adhesion level of rubber B on stainless steel surfaces 2B and 2D was about a tenth of the aforementioned reference values [74, 91].

Due to its geometry-independent nature, the single cantilever beam (SCB) test results are in principle comparable with the results found in literature. The average interfacial fracture energy values of the composite/rubber C interface ($\sim$260-440 J/m^2) are moderate when compared with corresponding values obtained for glass fibre reinforced epoxy/nickel-titanium interface ($\sim$2100 J/m^2 [92]) or for glass fibre reinforced thermoplastic/steel interface (850-1300 J/m^2 [93]). However, the nature of the interface and thus also the nature of the interfacial fracture is very different from the aforementioned references due to the elastic nature of the rubber. Here, the discussion of the SCB results concentrates on the inspections of the trends observed when varying rubber thickness or load rate.

The reason for the crack deflection from the steel/rubber interface towards the composite/rubber interface is assumed to be due to the higher strength of the steel/rubber joint when compared with the cohesive strength of the rubber. Thus the SCB results of the mild steel/rubber C interface remain at a qualitative stage for all rubber thicknesses and load rates and it can be only concluded that the mild steel/rubber C interface is stronger than the rubber's bulk properties. However, this is a good result that is in line with the peel test observations and reasserts the conclusion that the use of cohesive rubber strength instead of steel/rubber interfacial fracture energy in the simulations is possible.

For the composite/rubber C interface, an increasing trend in interfacial fracture energy with decreasing rubber thickness was observed. This agrees with the general observation that excessively thick adhesives result in poor strength, although ductile joints may perform better if the joint is a little thicker [62]. Thus, when aiming to high steel/composite bond strength, a thin rubber layer is preferred. This result together with the unstable crack growth of the samples with thick rubber layer implies that from an adhesion point of view, the thinner

the rubber layer, the higher strength for the steel/composite bond can be achieved. The instability of the crack in the thick rubber layer can be explained by the combined effect of the increased rubber thickness and different stress and energy states at the crack tip, which affect to the stability of the crack growth direction [93,94]. Although the effect of the rubber thickness could be studied only for the composite/rubber interface, it is assumed that the steel/rubber interface would have shown similar behaviour.

In the composite/rubber C interface, the interfacial fracture energy was found to increase with increasing load rate. In literature, the load rate dependency of interfacial fracture energy has been studied widely. In the review article of Cantwell and Blyton [95], it is concluded that for mode I (opening mode) fracture of brittle-matrix (e.g. epoxy) composites, the critical strain energy release rate G_{Ic} is either insensitive to or shows a slight increase with increasing load rate. In contrast, rubber modified epoxy composites show a reduction in G_{Ic} with increasing load rate [95]. For mode II fracture (sliding mode), the different studies reviewed in [95] show contradictory results, but the writers expect an increase in interlaminar fracture energy with increasing load rate both for tough and brittle-matrix composites. The SCB test induces a mixture of modes I and II and thus the results of the present study agree with the results found in literature.

In the case of bi-material systems, the strain rate dependency of the interlaminar fracture energy has been studied mainly with thermoplastic/metal systems. Examples of SCB test studies of bi-material interfaces are the ones of Reyes and Gupta [15], Cortés and Cantwell [96] and Reyes Villanueva *et al.* [97], who have studied the strain rate dependency of the interlaminar fracture energy. In these investigations, a clear increase in the interfacial fracture energy with increasing load rate [15, 97] or only a minor effect [96] was found for different thermoplastic/metal systems. The thermoset/steel samples of the current study showed an intermediate behaviour when compared with the aforementioned results. In addition, the results of the present study seem to refer to a linear effect of load rate on the interfacial fracture energy in the composite/rubber C interface (Fig. 7.2), but more load rates should be studied to validate this conclusion. For thermoplastic/aluminium interface, a linear behaviour has been observed in the load rate range 0.1-100 mm/min, beyond which the behaviour is non-linear [97]. Although the SCB tests were performed only for the mild steel/rubber C/composite structure, it can be assumed that similar behaviour would be observed for the stainless steel/rubber/composite hybrid structure as well.

The microscopy and adhesion test observations showed that the EPDM based rubbers can be used to create high quality stainless steel/epoxy composite hybrid structures. The microscopy studies showed that interfaces without discontinuities between the components can be achieved by the current manufacturing method. The peel test results of rubber A showed that a good, environmental resistant bond between stainless steel and fibre reinforced epoxy composite can be achieved by using a specific rubber as an adhesive. The pre-treatment requirements for the substrates are minimal, which makes the manufacturing of this kind of structures simple and easy. In addition, the estimation of the structure's strength can be done by using the knowledge of the rubber's bulk properties. According to the SCB tests, a thinner rubber layer provides higher interfacial fracture energy between the components. Thus, from the adhesion point of view, EPDM rubbers are very potential to be implemented in industrial applications as adhesives in stainless steel/fibre reinforced epoxy composite hybrid structures.

7.2 Dynamic properties of the steel/rubber/composite hybrid structures

The measured loss factor values for the plain mild steel and stainless steel sheets were around 0.005-0.01, which are in line with the loss factor values of steel found in literature ($2{\cdot}10^{-5}$-0.01 [81, 98, 99]). The loss factor of the composite appeared to be remarkably higher than that of the metal sheets, which was expected due to the more effective and versatile damping mechanisms of fibre reinforced composites. The damping mechanisms of composites include viscoelasticity, damping due to the fibre-matrix interface, thermoelastic damping due to the heat flow and damping due to damage [100] whereas the damping mechanisms of metals are microdefects, heat formation, corrosion, and damage initiation [101]. In addition, the frequency dependency of the composite's loss factor was stronger when compared with the steels.

The loss factor values of the mild steel/rubber C/composite hybrids were somewhat lower than the loss factors of the stainless steel/rubber B/composite based hybrids. Since there was no remarkable difference in the loss factor values of the cold rolled and stainless steel plates and as the composite sheets were similar in all the samples, the difference must arise from the higher loss factor of rubber B (Fig. 6.12). This result also emphasises the importance of the optimisation of rubber's physical properties when designing the structure for a specific application. In addition, especially in the case of stainless steel based hybrids, an increase in the loss factor with increasing rubber thickness can be seen. However, the effect of the rubbers to the loss factor of the structures' was small when compared with the effect of the composite.

It can be seen from Figs. 6.13 and 6.14 and from Table 6.3, that the use of volume fraction in the rule of mixtures (ROM) overestimates the loss factor results. Instead, the ROM results based on the use of the weight fractions seem to cohere better with the experimental results. The better suitability of the weight fraction instead of the volume fraction in the application of ROM is supposed to be due to the dominating nature of the steel sheets in the deformation of the hybrid structures. When volume fractions are used, the role of composite

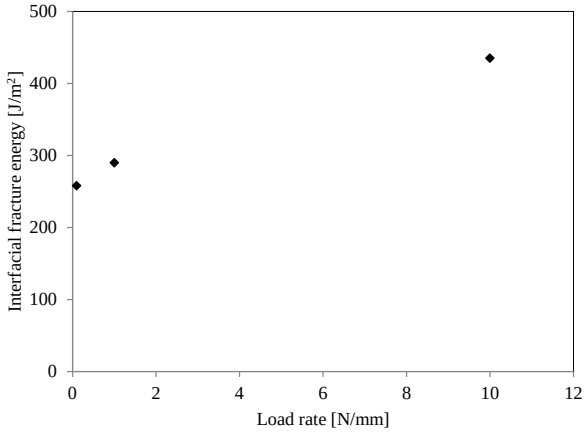

Figure 7.2: *Load rate versus interfacial fracture energy for composite/rubber C interface. Derived from the results of [Publication III].*

and rubber is emphasized whereas the role of steel sheet becomes more important due to its higher density if weight fractions are used. Since steel is much stiffer than composite or rubber, it dominates the elastic deformations of the hybrid structure and perhaps diminishes vibrations and damping in the other components. In addition, the energy lost E'' during deformation is the product of the loss factor η and modulus E' of the material (Eq. 7.1), which increases the importance of the stiff (high E') steel sheet further.

$$\eta = tan\delta = \frac{E''}{E'} \tag{7.1}$$

The ROM results seem to reproduce loosely the trends of the experimental loss factor results. Because the behaviour of the metal sheets and the rubber are not strongly frequency dependent within the measurement range, the similarity between the experimental data and the ROM estimation consolidates the assumption that the strong frequency dependency of the hybrids are rather due to the systematic effect of the composite's behaviour than measurement error. In addition, the effect of the composite in ROM estimation may be too low, as the ROM results are less frequency dependent than in the experimental data. Since the average loss factor values fitted so well with the experimental data, the effect of the interfacial damping mechanisms has to be small when compared with the damping capacity of the constituent materials. However, at certain measurement points, there is a noticeable positive or negative deviation in the experimental results from the ROM behaviour (Figs. 6.13 and 6.14). Thus, only the average loss factor of the steel/rubber/composite hybrids can be estimated by the ROM.

Table 7.1 represents a summary of the effect of the sample and test parameters on the high velocity impact behaviour of the studied steel/rubber/composite hybrid structures. In general, the effect of a change in the test parameters was stronger on the damage area than on the dissipated energy. The rubber thickness versus damage size studies showed that the rubber layer protects the structure from permanent damage. Even though the use of rubber does not change markedly the amount of absorbed energy, it obviously changes the energy absorption mechanisms: instead of causing failure in the composite layer, rubber absorbs the energy. Generally the energy is lost in viscous systems (such as in rubber) by heat build-up [102]. This change in the energy absorption mechanism can be seen in the decreased damage size. The 47% decrease in the damage area in the stainless steel based hybrid with 1.5 mm rubber B layer when compared with the epoxy based structure is a very promising result.

The overall deformation on the steel surface of hot samples was greater, which is supposed to be due to the softening of the rubber layer at high temperatures. The softening would allow easier plastic deformation of steel and thus higher energy dissipation during impacts. The increasing deviation with decreasing temperature of the composite damage area results may be due to the thermal stresses of the composite layer. The stress-free temperature of the composite is close to its cure temperature and the propensity for cracking towards colder temperatures is thus increased [103]. As in the adhesion studies, any effect of ageing on the impact properties of the stainless steel/rubber A/epoxy composite hybrid was not found.

Table 7.1: *A summary of the impact test results.*

Parameter	Damage area	Dissipated energy	Summary	Significance
Existence of rubber	*Clear decrease in the damage area when compared the rubber based samples to the epoxy adhesive based samples.*	*No effect.*	*Rubber protects the structure from permanent damage especially under repeated impacts.*	*Major variable in the design phase of steel/composite hybrid structures.*
Rubber thickness	*Decrease in the damage area with increasing rubber thickness.*	*No effect.*	*Thicker rubber protects the structure from permanent damage.*	*Major variable in the design phase of steel/rubber/composite hybrid structures.*
Sample temperature	*Slight increase in the damage area with increasing sample temperature.*	*Slight increase in the dissipated energy with increasing sample temperature.*	*The structure maintains its energy absorption ability at different temperatures without dramatic failure.*	*Minor variable in the design phase of steel/rubber/composite hybrid structures.*
Sample ageing	*No effect.*	*No effect.*	*Prior exposure to hot/moist environments does not affect the hybrid's behaviour.*	*Minor variable in the design phase of steel/rubber/composite hybrid structures.*
Impact energy	*Strong, linear increase in the damage area with increasing impact energy.*	*Slight increase in the dissipated energy with increasing impact energy.*	*The normal component of the impact energy has the most significant, linear effect on the hybrid's behaviour.*	*Major variable in the design phase of steel/rubber/composite hybrid structures.*

Continued on the next page

Table 7.1 – continued

Parameter	Damage area	Dissipated energy	Summary	Significance
Impact angle	*Strong, linear increase in the damage area with increasing impact angle.*	*Strong increase in the dissipated energy with increasing impact angle.*	*The normal component of the impact energy has the most significant, linear effect on the hybrid's behaviour.*	*Major variable in the design phase of steel/rubber/composite hybrid structures.*
Projectile velocity	*Slight increase in the damage area with increasing projectile velocity.*	*Slight increase in the dissipated energy with increasing projectile velocity.*	*At the studied range the effect of velocity is small*	*Minor variable in the design phase of steel/rubber/composite hybrid structures.*
Number of impacts	*The rubber based samples showed superior behaviour in comparison to the epoxy adhesive based samples. An increase in damage area with repeated impacts.*	*No effect*	*The structure maintains its ability to absorb energy without catastrophic failure even when the constituent layers or the interfaces have undergone damage.*	*Minor variable in the design phase of steel/rubber/composite hybrid structures.*

The linear dependency between the damage area and the normal component of the impact energy makes the evaluation of the stainless steel/rubber/composite hybrid structures' suitability for an industrial application easier. However, the relation between impact energy and absorbed energy are also important parameters to characterise the behaviour of materials [104] and these parameters can be compared in an energy profiling diagram (EPD). In Fig. 7.3a a schematic presentation of the typical EPD curve shape of a composite is shown. First, the absorbed energy growth slows down with increasing impact energy, until the projectile starts to penetrate into the sample. When the projectile penetrates into the sample and sticks into it, the EPD curve is at the equal energy line. Once the projectile perforates the sample, the absorbed energy does not any more increase with increasing impact energy. The EPD curve of stainless steel/rubber A/composite hybrid structure is shown in Fig. 7.3b and it can be seen that the shape of the hybrid's EPD curve is similar to the EPD curve of composite structures [104, 105].

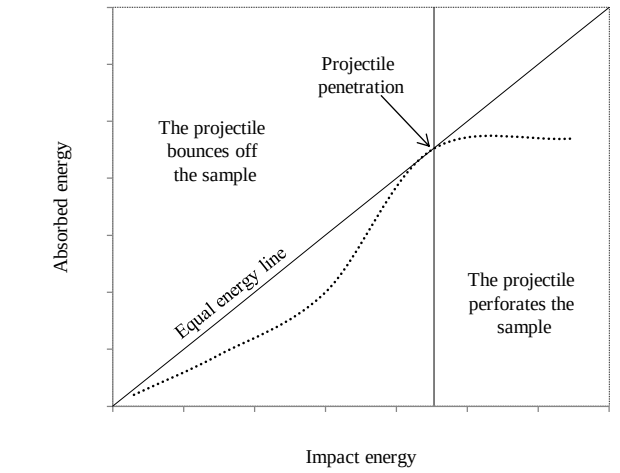

a)

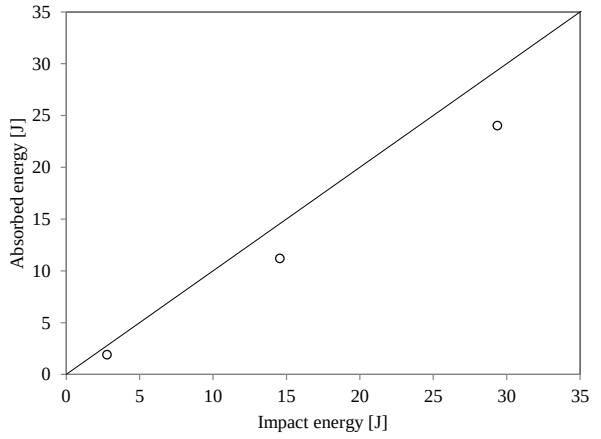

b)

Figure 7.3: *A schematic presentation of typical energy profile diagram (EPD) shape of composites in (a) and the EPD curve of the stainless steel/rubber A/composite hybrid structure (rubber thickness 1.0 mm) in (b).*

Impact angles closer to perpendicular angle induced more damage and higher level of penetration. It is assumed that at low angles, the surface steel exhibits more shear type loading, whereas at high angles the energy is increasingly consumed to more severe out-of-plane type plastic deformation in the surface steel. Especially applications where the material is exposed to erosion, the wear rate at low impact angles will be high regardless the good damping properties of the underlying composite structure. Yet, the results are promising even at high impact angles with relatively high impact energy since the present composite structure does not undergo catastrophic failure.

If only the normal component of the impact energy E_n is taken into account ($E_n = Esin(\theta)$ where E is the impact energy and θ is the impact angle, as in Fig. 7.4a), the results are linear, as shown in Fig. 7.4b. These results show that an increase in the impact angle has slightly stronger effect than an equivalent increase in the impact energy. If this kind of behaviour will be verified by further tests, it should be taken into account when evaluating the stress state and the suitability of the hybrid structure in an industrial application.

The observation that the sample impacted with the highest projectile velocity has a higher damage density although having similar energy absorption when compared with the intermediate projectile velocity agrees with the results of Chen and Ghosh [106]. They have simulated that for a certain microstructure, higher strain rate causes higher stress, which causes more damage. In general, the higher damage density further from the impacted surface, i.e. conical cross-sectional shape of impact damage, is typical for composite structures [107, 108] but it has been observed in other materials as well [109].

The multiple impact tests emphasised the positive effect of rubber on the damage tolerance of the structure. Since the energy absorbed does not change after repeated impacts, the degree of damage increases with increasing number of impacts. However, not only the sub-

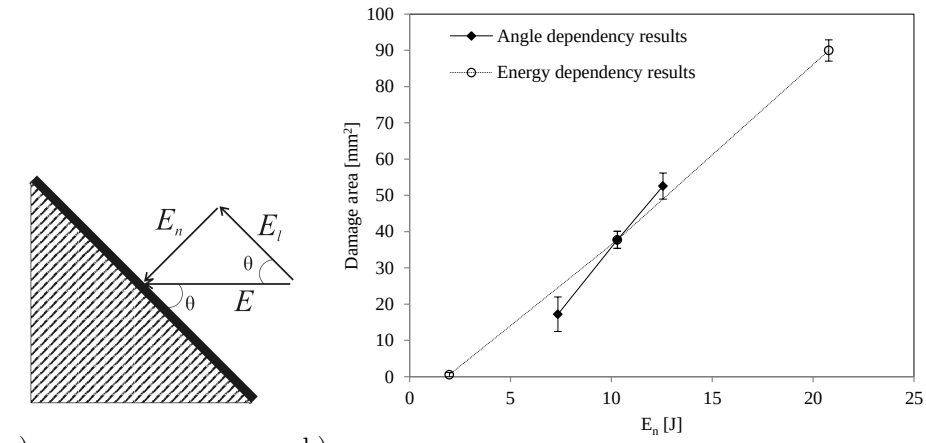

a) b)

Figure 7.4: *The impact angle θ, the impact energy E, the normal component of the impact energy E_n, and the in-plane component of the impact energy E_l are shown in (a). Figure (b) illustrates the damage areas versus the normal component of the impact energy for different impact angles and energies. [Unpublished]*

stantially smaller damage area but also the absence of delamination between the composite and rubber A showed that the rubber protects the structure from permanent damage. Since the energy absorption level remains at the same level, the hybrid structures have not lost their ability to bear dynamic loading even when the interface or the individual layers have undergone damage.

The scatter in the impact test results may have several origins. In addition to the error involved in the distance calculations (see Chapter 5.2), origins for the deviation of the test results are, for example, local variations in the rubber and/or composite thickness and the small variations in the tension of the clamp screws. For repeated impacts, the deviation increases with increasing number of impacts, but this can be explained by the slightly different projectile paths and impact positions.

The SEM studies showed that the first damages induced by high velocity impacts occurred in the composite layer. In addition, the highest density of individual failures in the highly damaged specimens was in the composite layers. These observations are in line with the vibration damping results which showed that from the hybrid's components the composite layer attenuates most effectively structural vibrations. Thus, from the energy absorption point of view, the composite layer has the most important effect on the hybrid's behaviour. This is partly due to the higher stake of composite when compared to the stake of the rubber in the studied hybrid structure. Anyhow, the impact tests showed that the rubber has an important role in improving the hybrid's damage tolerance. The finding that the density of fibre/matrix debonding was higher than the density of fibre breaks or matrix cracks implies that the fibre/matrix interface must be the weakest point of the composite. Still, the extent and the density of fibre/matrix debonding damages were surprisingly low in samples impacted with 3 J or 15 J, and thus it is assumed that the residual strength of the hybrid structures is not dramatically decreased. However, to ensure this assumption, compression after impact tests (CAI, ASTM D7137), for example, could be done, since the compressive strength is typically the limiting factor of composite materials in load bearing applications [110].

The difference in the impact crater size of the mild and stainless steel based hybrids can be attributed to the higher strength of the mild steel (yield strength 300 MPa [69]) compared with the stainless steel (yield strength 230 MPa [70]). In addition, the Shore D hardness of the rubbers may have had an effect on the crater size as well. The higher crater depth in the samples with a thick rubber layer can be explained by the higher deformability that the thicker rubber layer enables for the steel.

Only the use of rubber and changes in the normal component of the projectile's energy were found to have significant effect on the damage induced by high velocity impacts. Other sample and test set-up parameters had a minor effect. Similarly, the energy absorbed by the hybrid was mainly dependent on the normal component of the impact energy. Thus, these two impact event parameters should be concerned as the main variables when optimising, e.g. the rubber thickness, in the design phase.

When summing up the results of the adhesion and the impact test studies, it can be stated that rubber A showed very good adhesion to stainless steel and composite even after exposure to harsh environments. Thus a purpose-build rubber enables the manufacturing of stainless steel/composite hybrid structures which can, for example, replace all-metal solu-

tions and reduce the weight of the application. The use of stainless steel instead of mild steel provides corrosion resistance. The joint strength of these stainless steel/composite hybrids can be estimated by the cohesive strength of the purpose-built rubber.

Although the effect of the thin rubber layer on the vibration damping properties of the structure is small, it enables the replacement of all-metallic structures with a hybrid structure which has better vibration damping properties due to the composite. The damage tolerance of the rubber bonded stainless steel/composite hybrid under impact loading is clearly better when compared with a corresponding stainless steel/epoxy adhesive/composite structure. The protection against permanent failure was further improved by thicker rubber. Thus the rubber thickness should be optimized according to the required damping and damage tolerance level. The main findings and conclusions of this study are summarised in Fig. 7.5.

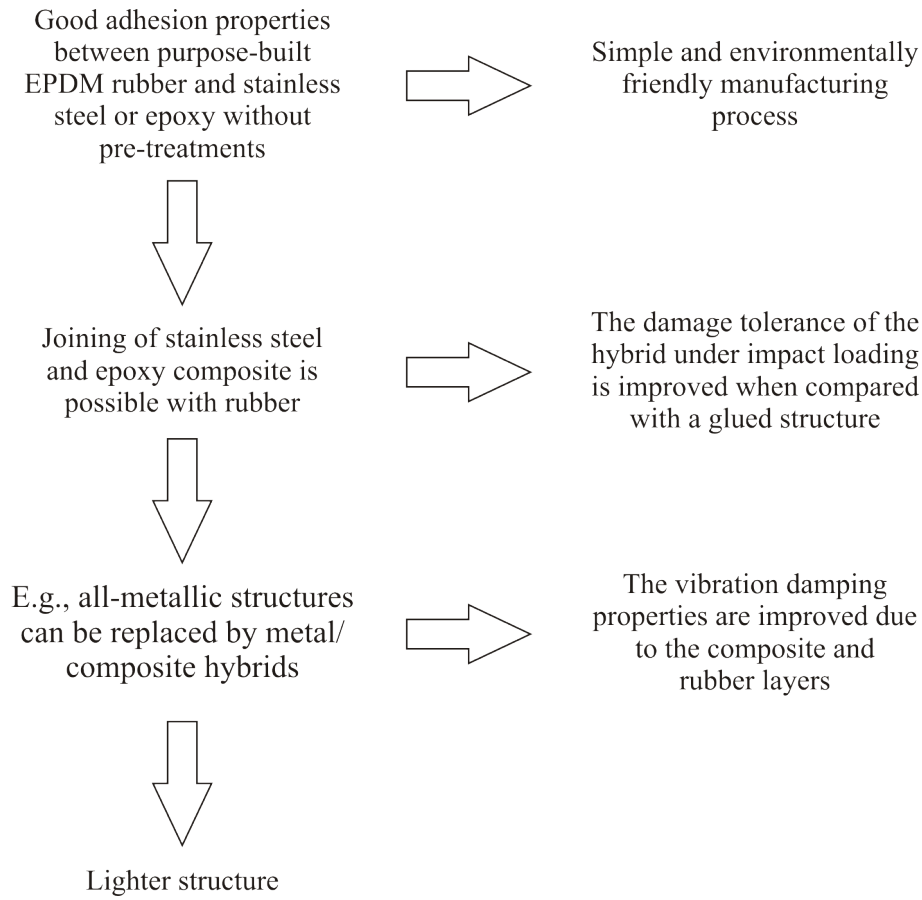

Figure 7.5: *A summary of the main findings and conclusions of this study.*

8 Concluding remarks

Hybrid structures combine the best properties of the constituent materials and can solve a wide range of design challenges faced today. The advantageous property combinations of hybrids can lead to valuable outcomes, such as reductions in energy consumption, cost efficiency, or improved functionalities. In this work, a new approach to join stainless steel and fibre reinforced epoxy composite by a thin ethylene propylene diene terpolymer (EPDM) based rubber layer is studied. Layered steel/rubber/composite hybrids were manufactured by vulcanising the rubber between the other components. Both adhesion properties and the energy absorption properties of the hybrids were tested in different environments.

The main findings and achievements of this study are the following results:

- A purpose-built EPDM rubber can be used to join stainless steel and epoxy composite without additional pre-treatments. The bond strength of the resulting hybrid structure is defined by the cohesive strength of the rubber and harsh hot/moist environments do not deteriorate the adhesion.
- The inclusion of composite with the aid of rubber improved the vibration damping properties of the hybrid structure significantly when compared to an all-metal structure.
- The EPDM rubber protects the structure from permanent damage when compared to a corresponding glued structure.

According to the electron microscopy studies, the manufacturing method proved to create well bonded interfaces without discontinuities between the components even when the rubber was applied on as-received stainless steel (surface finish standard 2B or 2D) and composite surfaces. Thus, rubber enables a straightforward and functioning manufacturing method of stainless steel/composite hybrids without time-consuming pre-treatments or adhesives. This is a major advantage when compared with the conventional joining procedures of polymers to stainless steel, which include several laborious manufacturing steps.

The adhesion tests showed that the joint strength of the hybrid structure can exceed the cohesive strength of the rubber. This enables the evaluation of the stainless steel/composite bond strength by using the bulk properties of the rubber instead of the substrate/rubber interfacial properties, which are difficult to define in a reliable manner. Also, according to the environmental testing, a steel/rubber/composite hybrid can maintain its adhesion properties even after exposure to harsh environments.

Due to the viscous nature of rubbers, also the energy absorption properties of the steel/rubber/composite hybrids were of interest. Under vibration excitation and high velocity impact loading the composite layer appeared to absorb most effectively energy among the different components of the hybrid. Thus, when compared to an all-metal structure, the hybrid exhibits significantly improved vibration damping properties. Weight fraction based rule of mixtures was applied successfully to evaluate the average vibration damping properties of the hybrid structure and the additional effect of the steel/rubber and composite/rubber

interfaces on the energy absorption properties was found to be small.

Although the use of rubber in the structure did not change markedly the hybrid's energy absorption properties, it had a significant effect on the extent of damage induced in the structure by dynamic loading. Under high velocity impact testing, the strongest effect on damage induced and energy absorbed was found to be the normal component of the projectile's energy. Also, higher rubber thickness led to less damage. Changes in the specimen temperature or in the frequency of vibration loading did not have a strong effect on the behaviour of the hybrid structure. Similar to the adhesion test results, ageing in harsh environments did not affect the dynamic properties. The samples maintained their ability to absorb energy even though the dynamic loading induced damage in the samples. These results indicate that apart from the good adhesion properties, rubber entails additional benefits, such as improved damage tolerance.

As a summation, it can be said that the studied approach to join stainless steel and fibre reinforced epoxy composite by EPDM based rubber has proven its ability to create well-bonded, environmentally resistant hybrid structures. Beside simple and straightforward manufacturing method, added value is gained in the form of improved damage tolerance under dynamic loading. Thus, this structure has high potential to be used in shell structures in industrial applications, such as in engine covers.

Despite the promising results of this study, there are still interesting and important aspects that should be investigated before the implementation of the structure in real-life applications. Although the current study showed that the stainless steel/rubber/composite structure withstands static hot/moist environments, cyclic testing with fluctuating temperature and/or humidity should be the next step towards more realistic and demanding test conditions. Further studies on this topic would not only offer essential information for the development of steel/rubber/composite hybrids but also expand the knowledge of the behaviour of the interfaces in organic/inorganic bi-materials.

In addition to further studies, the optimisation of the hybrid's components has to be done before the implementation of the structure. Steel grade, rubber polymer(s) and additives, composite fibres and matrix as well as the component thicknesses have to be chosen to meet the requirements of the specific application.

The test methods used in this study were chosen to correspond the possible load environment of shell structures. However, if this stainless steel/rubber/composite hybrid structure would be used in a different type of application, e.g. as a load-bearing component, it should also be tested in a different way. For example, three-point bend test and tensile test could be then relevant test methods. In addition to further mechanical testing of the hybrid structure, its modelling and simulation are essential steps before the structure can be adopted in large scale industrial components. Further, the whole life cycle of the hybrid has to be known and, by implication, also the recyclability of the structure has to be considered.

Although there are several topics around the stainless steel/rubber/composite hybrid structure which would be interesting to study further, the current study has shown that this new approach to join stainless steel and epoxy composites by EPDM based rubber has potential to be further developed and to be considered as a lighter, corrosion resistant option to shell structures in many different fields of industry.

Bibliography

[1] M. Ashby. Hybrid materials to expand the boundaries of material-property space. *Journal of the American Ceramic Society*, 94:s3–s14, 2011.

[2] S. T. Amancio-Filho and J. F. dos Santos. Joining of polymers and polymer-metal hybrid structures: Recent developments and trends. *Polymer Engineering & Science*, 49(8):1461–1476, 2009.

[3] A. Baldan. Review: Adhesively-bonded joints in metallic alloys, polymers and composite materials: Mechanical and environmental durability performance. *Journal of Materials Science*, 39:4729–4797, 2004.

[4] S. Minett and K. A. Fenwick. A steel-rubber laminate that can quieten cars & other machines. *Noise & Vibration Worldwide*, 30(2):12–13, 1999.

[5] I-Car Advantage Online. Laminated steel. [www] [June 2013] http://www.i-car.com.

[6] Paragon Manufacturing Inc. Quiet equates to quality. [www] [June 2013] http://www.noisedamp.com/.

[7] Arcelor Mittal. Sollight user manual. [www] [June 2013] http://www.constructalia.com.

[8] M. Grujicic, V. Sellappan, G. Arakere, N. Seyr, A. Obieglo, M. Erdmann, and J. Holzleitner. The potential of a clinch-lock polymer metal hybrid technology for use in load-bearing automotive components. *Journal of Materials Engineering and Performance*, 18(7):893–902, 2009.

[9] LANXESS. Hybrid technology. [www] [June 2013] http://techcenter.lanxess.com.

[10] O. J. Zoellner and J. A. Evans. Plastic-metal hybrid: A new development in the injection molding technology. In *Proceedings of SPE Annual Technical Conference (ANTEC)*, San Francisco, CA, USA, 2002.

[11] C. A. J. R. Vermeeren. An historic overview of the development of fibre metal laminates. *Applied Composite Materials*, 10(4-5):189–205, 2003.

[12] F. Plenk and J. Schaube. Rubberize your composites - Simple integration of new features in fiber reinforced plastics (FRP). In *Proceedings of SAMPE Europe 30th International Jubilee Conference and Forum*, Paris, France, 2009.

[13] L. B. Vogelesang and A. Vlot. Development of fibre metal laminates for advanced aerospace structures. *Journal of Materials Processing Technology*, 103(1):1–5, 2000.

[14] S. H. Song, Y. S. Byun, T. W. Ku, W. J. Song, J. Kim, and B. S. Kang. Experimental and numerical investigation on impact performance of carbon reinforced aluminum laminates. *Journal of Materials Science & Technology*, 26(4):327–332, 2010.

[15] G. Reyes and S. Gupta. Manufacturing and mechanical properties of thermoplastic hybrid laminates based on DP500 steel. *Composites Part A: Applied Science and Manufacturing*, 40(2):176–183, 2009.

[16] R. G. J. van Rooijen, J. Sinke, and S. van der Zwaag. Improving the adhesion of thin stainless steel sheets for fibre metal laminate (FML) applications. *Journal of Adhesion Science and Technology*, 19(16):1387–1396, 2005.

[17] D. A. Burianek and S. M. Spearing. Fatigue damage in titanium-graphite hybrid laminates. *Composites Science and Technology*, 62(5):607–617, 2002.

[18] M. Weiss, B. F. Rolfe, M. Dingle, and J. L. Duncan. Elastic bending of steel-polymer-steel (SPS) laminates to a constant curvature. *Journal of Applied Mechanics*, 73(4):574–579, 2006.

[19] Y.-M. Huang and D.-K. Leu. Finite-element simulation of the bending process of steel/polymer/steel laminate sheets. *Journal of Materials Processing Technology*, 52(24):319–337, 1995.

[20] A. Carrad, J. Faerber, S. Niemeyer, G. Ziegmann, and H. Palkowski. Metal/polymer/metal hybrid systems: Towards potential formability applications. *Composite Structures*, 93(2):715–721, 2011.

[21] Arcelor Mittal. Steel roofing: Timeless aesthetic quality. [www] [June 2013] http://www.constructalia.com.

[22] S. Bistac, M. F. Vallat, and J. Schultz. Investigation of chemical interactions at the steel/polymer interface by FT-IR diffuse reflectance spectroscopy. *Applied Spectroscopy*, 51(12):1823–1825, 1997.

[23] M. Grujicic, V. Sellappan, M. A. Omar, N. Seyr, A. Obieglo, M. Erdmann, and J. Holzleitner. An overview of the polymer-to-metal direct-adhesion hybrid technologies for load-bearing automotive components. *Journal of Materials Processing Technology*, 197(13):363–373, 2008.

[24] G. Lucchetta, F. Marinello, and P. F. Bariani. Aluminum sheet surface roughness correlation with adhesion in polymer metal hybrid overmolding. *CIRP Annals - Manufacturing Technology*, 60(1):559–562, 2011.

[25] M. Grujicic, V. Sellappan, S. Kotrika, G. Arakere, A. Obieglo, M. Erdmann, and J. Holzleitner. Suitability analysis of a polymer-metal hybrid technology based on high-strength steels and direct polymer-to-metal adhesion for use in load-bearing automotive body-in-white applications. *Journal of Materials Processing Technology*, 209(4):1877–1890, 2009.

[26] M. Grujicic, V. Sellappan, T. He, N. Seyr, A. Obieglo, M. Erdmann, and J. Holzleitner. Total life cycle-based materials selection for polymer metal hybrid body-in-white automotive components. *Journal of Materials Engineering and Performance*, 18(2):111–128, 2009.

[27] H. L. Gower. *Welding of a metal-polymer laminate*. PhD thesis, Delft University of Technolog, The Netherlands, 2007.

[28] M. Weiss, B. F. Rolfe, M. E. Dingle, and P. D. Hodgson. The influence of interlayer thickness and properties on spring-back of SPS- (Steel/Polymer/Steel) laminates. *Steel Grips*, 2:445–449, 2004.

[29] I. Burchitz, R. Boesenkool, S. van der Zwaag, and M. Tassoul. Highlights of designing with Hylite - a new material concept. *Materials & Design*, 26(4):271–279, 2005.

[30] ThyssenKrupp Stahl. BONDAL composite material with structure-borne sound damping properties. [www] [June 2013] http://www.thyssenkrupp-steeleurope.com.

[31] M. A. Ansarifar, J. Zhang, J. Baker, A. Bell, and R. J. Ellis. Bonding properties of rubber to steel, aluminium and nylon 6,6. *International Journal of Adhesion and Adhesives*, 21(5):369–380, 2001.

[32] M. A. Ansarifar, J. Zhang, A. Bell, and R. J. Ellis. Role of primer in rubber to nylon 6,6 bonding. *International Journal of Adhesion and Adhesives*, 22(3):245–255, 2002.

[33] R. Wiering. Damage development of Glare laminates under impact conditions. [www] [June 2013] http://www.utwente.nl.

[34] Airbus. A380 Family. [www] [November 2013] http://www.airbus.com/.

[35] The Neue Materialien Fürth GmbH. Hybrid technology. [www] [July 2013] http://www.new-materials.de.

[36] Audi. A8. [www] [November 2013] http://www.audi.com/.

[37] Minor rubber. Products. [www] [July 2013] http://www.minorrubber.com/.

[38] Sandvik. Products. [www][November 2013] http://www.sandvik.com.

[39] C. Bähr, E. Stammen, R. Thiele, S. Böhm, K. Dilger, and J. Büchs. Withstanding frequent steam sterilisation: Innovative technique to bond glass and stainless steel composites in biotechnology and endoscopic medicine. *International Journal of Adhesion and Adhesives*, 33:15–25, 2012.

[40] J. Cognard. Some recent progress in adhesion technology and science. *Comptes Rendus Chimie*, 9(1):13–24, 2006.

[41] H. Yamabe. Stabilization of the polymer-metal interface. *Progress in Organic Coatings*, 28(1):9–15, 1996.

[42] G. Lothongkum, S. Chaikittisilp, and A. W. Lothongkum. XPS investigation of surface films on high Cr-Ni ferritic and austenitic stainless steels. *Applied Surface Science*, 218(1-4):202–209, 2003.

[43] M. A. Perez, R. D. Waid, J. E. Gozum, C. L. S. Elsbernd, and M. D. Gehlsen. *Thermoplastic/thermoset hybrid foams and methods for making same.* US6323251 Patent, 27.11.2001.

[44] B. Crowther. *Handbook of rubber bonding.* Smithers Rapra Technology, Shrewsbury, UK, 2001.

[45] K. Mequanint, R. Sanderson, and H. Pasch. Adhesion properties of phosphate- and siloxane-containing polyurethane dispersions to steel: An analysis of the metal-coating interface. *Journal of Applied Polymer Science*, 88(4):900–907, 2003.

[46] J. L. Delattre, R. dAgostino, and F. Fracassi. Plasma-polymerized thiophene films for enhanced rubber-steel bonding. *Applied Surface Science*, 252(10):3912–3919, 2006.

[47] F. Bouquet, J. M. Cuntz, and C. Coddet. Influence of surface treatment on the durability of stainless steel sheets bonded with epoxy. *Journal of Adhesion Science and Technology*, 6(2):233–242, 1992.

[48] J. R. J. Wingfield. Treatment of composite surfaces for adhesive bonding. *International Journal of Adhesion and Adhesives*, 13(3):151–156, 1993.

[49] M. Kanerva and O. Saarela. The peel ply surface treatment for adhesive bonding of composites: A review. *International Journal of Adhesion and Adhesives*, 43:60–69, 2013.

[50] R. Brown. *Physical testing of rubber*. Springer, New York, USA, 2006.

[51] R. Simpson. *Rubber basics*. Smithers Rapra Technology, Shrewsbury, UK, 2002.

[52] B. Rodgers. *Rubber compounding chemistry and applications*. Marcel Dekker Inc., New York, USA, 2004.

[53] Y. Chokanandsombat, P. Sea-Oui, and C. Sirisinha. Experimental investigation of the stress-stretch behavior of EPDM rubber with loading rate effects. *Advanced Materials Research*, 747:471–474, 2013.

[54] Sah Petroleums Limited. rubber process oils. [www] [November 2013] http://www.sahpetroleums.com.

[55] W. H. Charch. *Laminated structure and method for preparing same*. US2128635 Patent, 23.3.1935.

[56] W. Nagel. Techniques for bonding rubber to metal using metallic coagents. *Rubber World*, (1), November 1998.

[57] Cray Valley USA, LLC. Technical data sheet: Ricobond 2031. [www] [June 2013] http://www.crayvalley.com.

[58] Sartomer Company, Inc. Technical data sheet: Saret SR 633. [www] [May 2013] http://www.gmzinc.com.

[59] Cray Valley USA, LLC. Technical data sheet: Dymalink 633. [www] [June 2013] http://www.crayvalley.com.

[60] 3M. Products. [www] [June 2013] http://www.3m.com/.

[61] Elmer's Products, Inc. Technical data sheet: Ross rubber cement glue (latex). [www] [June 2013] http://www.elmers.ca.

[62] D. E. Packham. *Handbook of Adhesion*. John Wiley & Sons, West Sussex, England, 2 edition, 2005.

[63] W. Hofman. *Rubber technology handbook*. Hanser/Gardner Publications, Cincinnati, USA, 3 edition, 1996.

[64] International rubber study group. Statistics. [www][July 2013] http://www.rubberstudy.com.

[65] International Institute for Procurement & Marker Research. Global demand for EPDM (ethylene propylene diene monomer) is set to increase by 1.5 million tons by 2020. [www] [April 2013] http://iipmr.com.

[66] M. Cheng and W. Chen. Experimental investigation of the stress-stretch behavior of EPDM rubber with loading rate effects. *International Journal of Solids and Structures*, 40(18):4749–4768, 2003.

[67] International Institute of Synthetic Rubber Producers, Inc. Ethylene-Propylene Rubbers & Elastomers. [www] [April 2013] http://www.iisrp.com.

[68] The australian stainless steel development association (ASSDA). Stainless steel. [www] [June 2013] http://www.assda.asn.au/.

[69] Ruukki. Cold rolled steels. [www][June 2013] http://www.ruukki.com.

[70] Outokumpu. Stainless steel. [www] [June 2013] http://www.outokumpu.com.

[71] B. Song and W. Chen. Dynamic compressive behaviour of EPDM rubber under nearly uniaxial strain conditions. *Journal of Engineering Materials and Technology*, 126:213–217, 2004.

[72] Matrix Composite Materials Company Ltd. Product data sheets - Epoxy. [www] [October 2013] http://www.matrix-composites.co.uk.

[73] A. Ciecielski. *An introduction to rubber technology.* Smithers Rapra Technology, Shrewsbury, UK, 1999.

[74] J. W. Cook, S. Edge, and D. E. Packham. The adhesion of natural rubber to steel and the use of the peel test to study its nature. *International Journal of Adhesion and Adhesives*, 17(4):333–337, 1997.

[75] J. K. L. Mittal. *Adhesion measurement of films and coatings*, volume 2. VSP - An imprint of BRILL, Zeist, the Netherlands, 2001.

[76] M. Kenane and M. L. Benzeggagh. Mixed-mode delamination fracture toughness of unidirectional glass/epoxy composites under fatigue loading. *Composites Science and Technology*, 57(5):597–605, 1997.

[77] Jedec solid state technology association. Steady state temperature humidity bias life test. *JESD22-A101C*, 2009.

[78] D. J. Ewins. *Modal testing: theory, practice, and application.* Research Studies Press, 2 edition, 2000.

[79] Y. Liu, M. Zogg, and P. Ermanni. An experimental comparative study on non-conventional surface and interface damping techniques for automotive panel structures. *Journal of Vibration and Control*, 18(14):2210–2233, 2012.

[80] M. Matter, T. Gmür, J. Cugnoni, and A. Schorderet. Identification of the elastic and damping properties in sandwich structures with a low core-to-skin stiffness ratio. *Composite Structures*, 93(2):331–341, 2011.

[81] C. Harris and A. Piersol, editors. *Harris' shock and vibration handbook.* McGraw-Hill, New York, USA, 2002.

[82] M. Apostol, V.-T. Kuokkala, A. Laukkanen, K. Holmberg, R. Waudby, and M. Lindroos. High velocity particle impactor modelling and experimental verification of impact wear tests. In *Proceedings of the World Tribology Congress*, Torino, Italy, 2013.

[83] J. M. Kelly and D. Konstantinidis. *Mechanics of rubber bearings for seismic and vibration isolation.* Wiley, Somerset, USA, 2011.

[84] R. M. Silverstein and F. X. Webster. *Spectrometric identification of organic compounds*. John Wiley & Sons, New York, USA, 6 edition, 1997.

[85] J.-P. Pascault, H. Sautereau, J. Verdu, and R. J. J. Williams. *Thermosetting polymers*. CRC Press, New York, USA, 2002.

[86] S. Ebnesajjad and C. Ebnesajjad, editors. *Surface Treatment of Materials for Adhesive Bonding*. William Andrew, Norwich, NY, USA, 2006.

[87] K. Ozawa, T. Kakubo, K. Shimizu, N. Amino, K. Mase, Y. Izumi, T. Muro, and T. Komatsu. High-resolution photoelectron spectroscopy study of degradation of rubber-to-brass adhesion by thermal aging. *Applied Surface Science*, 268:117–123, 2013.

[88] T. C. Chivers and A. F. Georgen. EPDM and uorocarbon seal materials: a comparison of performance for nuclear fuel transport asks. In *Proceedings of 14th International symposium on the packaging and transport of radioactive materials*, Berlin, Germany, 2004.

[89] S. J. Metz. *Water vapor and gas transport through polymeric membranes*. PhD thesis, University of Twente, The Netherlands, 2003.

[90] J. A. Williams and J. J. Kauzlarich. The influence of peel angle on the mechanics of peeling flexible adherends with arbitrary load-extension characteristics. *Tribology International*, 38:951–958, 2005.

[91] M. Honkanen, M. Hoikkanen, M. Vippola, J. Vuorinen, and T. Lepistö. Metal-plastic adhesion in injection-molded hybrids. *Journal of Adhesion Science and Technology*, 23:1747–1761, 2009.

[92] P. Cortés, W. J. Cantwell, and K. S. C. Kuang. The fracture properties of a smart fiber metal laminate. *Polymer Composites*, 28(4):534–544, 2007.

[93] B. Chen and D. A. Dillard. Numerical analysis of directionally unstable crack propagation in adhesively bonded joints. *International Journal of Solids and Structures*, 38:6907–6924, 2001.

[94] M. T. Tilbrook, K. Rozenburg, E. D. Steffler, L. Rutgers, and M. Hoffman. Crack propagation paths in layered, graded composites. *Composites Part B: Engineering*, 37:490–498, 2006.

[95] W. Cantwell and M. Blyton. Influence of loading rate on the interlaminar fracture properties of high performance composites - A review. *Applied Mechanics Reviews*, 52(6):199–212, 1999.

[96] P. Cortés and W. J. Cantwell. Interfacial fracture properties of carbon fiber reinforced PEEK/titanium fiber-metal laminates. *Journal of Materials Science Letters*, 21:1819–1823, 2002.

[97] G. Reyes Villanueva, W. J. Cantwell, J. Cruz M., and F. A. Velasco A. The impact properties of novel thermoplastic-based fibre-metal laminates. In *Proceedings of VI International Conference on Composite Materials*, Morelia, Mexico, 2003.

[98] Irvine T. Damping properties of materials, Revision c. [www] [June 2013] http://syont.files.wordpress.com.

[99] T. Allgeier, R. D. Adams, and W. T. Evans. Vibrational measurement of the specific damping capacity of 15-5 ph stainless steel. *Proceedings of the Institution of Mechanical Engineers*, 211(1):49–53, 1997.

[100] R. Chandra, S. P. Singh, and K. Gupta. Damping studies in fiber-reinforced composites A review. *Composite Structures*, 46(1):41–51, 1999.

[101] E. C. Botelho, A. N. Campos, E. de Barros, L. C. Pardini, and M. C. Rezende. Damping behavior of continuous fiber/metal composite materials by the free vibration method. *Composites Part B: Engineering*, 37(23):255–263, 2006.

[102] E. E. Ungar. Damping of structures and use of damping materials. In M. J. Crocker, editor, *Handbook of Noise and Vibration Control*, pages 734–744. John Wiley & Sons, Hoboken, New Jersey, USA, 2007.

[103] B. S. Hayes and L. M. Gammon. *Optical Microscopy of Fiber-Reinforced Composites*. ASM International, page 160, 2010.

[104] M. Sayer, N. M. Bektaş, and O. Sayman. An experimental investigation on the impact behaviour of hybrid composite plates. *Composite Structures*, 92:1256–1262, 2010.

[105] G. Belingardi, M. P. Cavatorta, and D. S. Paolino. On the rate of growth and extent of the steady damage accumulation phase in repeated impacts. *Composites Science and Technology*, 69:1693–1698, 2009.

[106] Chen Y. and Ghosh S. Micromechanical analysis of strain rate-dependent deformation and failure in composite microstructures under dynamic loading conditions. *International Journal of Plasticity*, 32–33:218–247, 2012.

[107] M. V. Hosur, M. R. Karim, and Jeelani S. Experimental investigations on the response of stitched/unstitched woven S2-glass/SC15 epoxy composites under single and repeated low velocity impact loading. *Composite Structures*, 61:89–102, 2003.

[108] R. Olsson. Analytical model for small mass impact with delamination growth. In *Proceedings of the 17th International Conference on Composite Materials*, Edinburgh, UK, 2009.

[109] S. M. Walley, J. E. Field, and P. Yennadhiou. Single solid particle impact erosion damage on polypropylene. *Wear*, 100:263–280, 1984.

[110] C. R. Schultheisz and A. M. Waas. Compressive failure of composites, Part I: Testing and micromechanical theories. *Progress in Aerospace Sciences*, 32:1–42, 1996.

Tampereen teknillinen yliopisto
PL 527
33101 Tampere

Tampere University of Technology
P.O.B. 527
FI-33101 Tampere, Finland

ISBN 978-952-15-3278-8
ISSN 1459-2045